Mon. Not. R. Astron. Soc. **000**, 000–000 (0000) Printed 15 September 2015 (MN LATEX style file v2.2)

Variability of QSOs with variable regions in broad absorption troughs from the Sloan Digital Sky Survey

Zhi-Cheng He, Wei-Hao Bian*, Xiao-Lei Jiang and Xue Ge
Department of Physics and Institute of Theoretical Physics, Nanjing Normal University, Nanjing 210023, China

15 September 2015

ABSTRACT
The variability of broad absorption lines is investigated for a sample of 188 broad-absorption-line (BAL) quasars (QSOs) ($z > 1.7$) with at least two-epoch observations from the Sloan Digital Sky Survey Data Release 7 (SDSS DR7), covering a time-scale of about 0.001 – 3 years in the rest frame. Considering only the longest time-scale between epochs for each QSO, 73 variable regions in the C IV BAL troughs are detected for 43 BAL QSOs. The proportion of BAL QSOs showing variable regions increases with longer time-interval than about 1 year in the rest frame. The velocity width of variable regions is narrow compared to the BAL-trough outflow velocity. For 43 BAL QSOs with variable regions, it is found that there is a medium strong correlation between the variation of the continuum luminosity at 1500 Å and the variation of the spectral index. With respect to the total 188 QSOs, larger proportion of BAL QSOs with variable regions appears bluer during their brighter phases, which implies that the origin of BAL variable regions is related to the central accretion process. For 43 BAL QSOs with variable regions, it is possible that there is a negative medium strong correlation between the absolute variation of the equivalent width and the Mg II -based black hole mass, and a medium strong correlation between the maximum outflow velocity of variable regions and the Eddington ratio. These results imply the connection between the BAL-trough variation and the central accretion process.

Key words: galaxies:active—galaxies:nuclei—quasars:absorption lines

1 INTRODUCTION

Broad absorption line quasars (BAL QSOs) exhibit broad absorption troughs for high-ionization ultraviolet (UV) lines such as Si IV 1399, C IV 1549, C III] 1909 (known as HiBAL), or/and low-ionization UV lines such as Mg II 2799 (known as LoBAL). BAL QSOs were usually identified from their UV spectra by the balnicity index (BI), considering different BAL outflow velocity and/or BAL velocity width (e.g. Weymann et al. 1991; Trump et al. 2006; Gibson et al. 2009; He et al. 2014). BAL troughs are present in about 10-40% of QSOs (e.g. Gibson et al. 2009; Allen et al. 2011).

BAL troughs in QSOs are thought to be the strongest observed signature of QSO winds (Fabian 2012). One explanation for BALs is an orientation-dependent effect, where QSOs appear as BAL QSOs when the disk wind is on the line of sight (e.g. Murray et al. 1995; Elvis 2002). The requirement that detection of a wind should be orientation-dependent is very similar to the case of other structures in QSOs, such as the broad-line region (BLR) or jet (e.g. Urry & Padovani 1995). Another explanation for BALs is an orientation-independent evolution effect (e.g. Gibson et al. 2008; Zubovas & King 2013). As an evolutionary stage of active galactic nucleus (AGN), the expulsion of gas and dust by galaxy collision possibly causes the BAL outflows. It was supported by no correlations exist between outflow properties and orientation, such as the similar range of viewing angles for radio-loud BALs and radio-loud non-BALs (e.g. Fine et al. 2011; Bruni et al. 2012).

The disk wind in BAL QSOs is believed to come from the central supermassive black hole (SMBH) accretion disc, and BAL region often lies outside the BLR region (e.g. Proga et al. 2000; Murray et al. 1995; Filiz Ak et al. 2013). There exists an empirical relation between the BLR size and the continuum luminosity in AGN/QSOs (e.g. Kaspi et al. 2005; Bentz et al. 2009). For the BAL region outside of BLR region, larger luminosity would lead to larger size, smaller orbital velocity of the BAL regions. It would lead the properties/variability of BAL outflows as a function of luminosity. The wind dependence on the properties of QSOs has been discussed by many authors, suggesting the connection between the outflow and the accretion process (e.g. Laor & Brandt 2002; Ganguly et al. 2007; Baskin & Laor 2013; He et al. 2014). It was found that the maximum outflow velocity increases with both the bolometric luminosity and the blueness of the spectral slope, suggesting the idea of radiation-pressure-driven outflows (Laor & Brandt 2002; Ganguly et al. 2007). At the same time, BAL-troughs often vary over rest-frame time-

* E-mail: whbian@njnu.edu.cn

scales of days to years, which can provide clues to the origin of BAL QSOs (e.g. Gibson et al. 2008; Capellupo et al. 2011, 2012, 2013; Filiz Ak et al. 2012, 2013; Grier et al. 2015). Capellupo et al. (2011, 2012, 2013) investigated BAL variability for 24 QSOs with long time-scales and multiple epochs. They found that variability typically occurs only in portions of the BAL troughs; the components at higher outflow velocities are more likely to vary than those at lower velocities and weaker BALs are more likely to vary than stronger BALs; both the incidence and the amplitude of variability are greater across longer time-scales. With a sample of 291 BAL QSOs from SDSS-I/II/III, Filiz Ak et al. (2013) investigated BAL variations as a function of QSOs properties and did not find significant evidence for correlations between BAL variability and luminosity/Eddington ratio/SMBH mass. For C IV 1549 troughs on moderate time-scales (1-2.5 yrs), they suggested possible correlations between BAL variability and luminosity/Eddington ratio. Filiz Ak et al. (2013) used C IV emission line to calculate the SMBH mass and the Eddington ratio, which have larger scatters and bias compared to that by other emission lines such as Hβ , Mg II .

For some samples of QSOs, it has been shown that spectra of QSOs at low redshifts are bluer during their brighter phases (e.g. Wilhite et al. 2005; Pu et al. 2006; Meusinger et al. 2011; Zuo et al. 2012; Bian et al. 2012a). The trend of bluer spectra during brighter phases is usually explained by the accretion variation. During the brighter phase, the accretion disk becomes hotter and its emission peak would move to shorter wavelengths (big blue bump), which would also lead to larger variance in the blue spectrum. However, other contributions may mingle in this kind of investigation, such as the contribution of UV/optical Fe II , Balmer continuum, jet, and the host, as well as the complex of accretion disk model. With two-epoch variation, it was found that the spectra of half of the QSOs appear redder during their brighter phases (Bian et al. 2012a; Guo & Gu 2014).

The feature of variable regions in BAL-trough were investigated by some authors (e.g. Gibson et al. 2008; Filiz Ak et al. 2012, 2013). Using a sample of 13 BAL QSOs with two-epoch spectra covering 3-6 years in the rest frame, Gibson et al. (2008) identified the variable regions in BAL-trough and investigated the variation of C IV BAL-trough between the Large Bright Quasar Survey (LBQS; Hewett et al. 1995) and the Sloan Digital Sky Survey (SDSS). With SDSS/Baryon Oscillation Spectroscopic Survey (BOSS), we have investigated the relation between the wind and QSO properties for a single BAL QSO with 18 epochs observations covering about 3 years in the rest frame (He et al. 2014). Here, we present a sample of 188 BAL QSOs with at least two-epoch observation from SDSS Data Release 7 (DR7). This sample is used to investigate the feature of the BAL-trough variable regions, the variability of UV spectral index and the BAL-trough equivalent width (EW), as well as the relation with the central accretion properties. Section 2 presents the sample. Section 3 gives the spectral analysis. Section 4 contains our results and discussion. A summery is given in the last section. Throughout this work, we use a cosmology with $H_0 = 70 \mathrm{km\,s^{-1}Mpc^{-1}}$, $\Omega_M = 0.3$, and $\Omega_\Lambda = 0.7$.

2 THE SAMPLE OF C IV BAL QSOS WITH TWO-EPOCH OBSERVATIONS FROM THE SDSS DR7

The SDSS DR7 (York et al. 2000) contains imaging of almost 11663 $\mathrm{deg^2}$ and spectra for roughly 93×10^4 galaxies and 12×10^4 QSOs, observed by 2.5 m telescope at the Apache Point Observatory in New Mexico. The SDSS spectra were obtained through 3" fibers. For the SDSS DR7 spectra, the observational wavelength coverage is from 3800 Å to 9200 Å, and the spectral resolution is $1850-2200$. With SDSS DR7, Shen et al. (2011) gave a compilation of properties of 105783 QSOs. With the modified balnicity index $\mathrm{BI_0}$ ($0\ \mathrm{km\ s^{-1}}$ as a minimum detection limit for the outflow velocity range), there are 6214 BAL QSOs identified in their SDSS DR7 sample. It is found that there are 1080 spectra of 480 C IV BAL QSOs with at least two-epoch observations. In order to identify the variable regions in C IV BAL troughs, we select BAL QSOs with SDSS spectral signal-to-noise ratio (S/N) at r band larger than 10, and redshift more than 1.7. It is consist of 188 C IV BAL QSOs with 428 SDSS spectra. For each QSO with more than two epochs, we consider only the longest time-scale between two epochs. In Fig. 1, we give the S/N versus the redshift, and the luminosity at 1350Å (L_{1350}) versus the spectral MJD values. The stars denote 480 C IV BAL QSOs with at least two-epoch observations, and the blue circles denote our 188 C IV BAL QSOs with longest two-epoch SDSS spectra with S/N(r) $>$ 10 and z$>$1.7. In Fig. 1, for our sample of 188 BAL QSOs, the redshift distribution is between 1.7 and about 3.9, the S/N distribution is between 10 and about 60. Considering the problem of spectrophotometric flux calibration for BOSS in SDSS III, we just use the spectra from SDSS DR7 (e.g. Paris et al. 2014; Margala et al. 2015). Our sample is different to

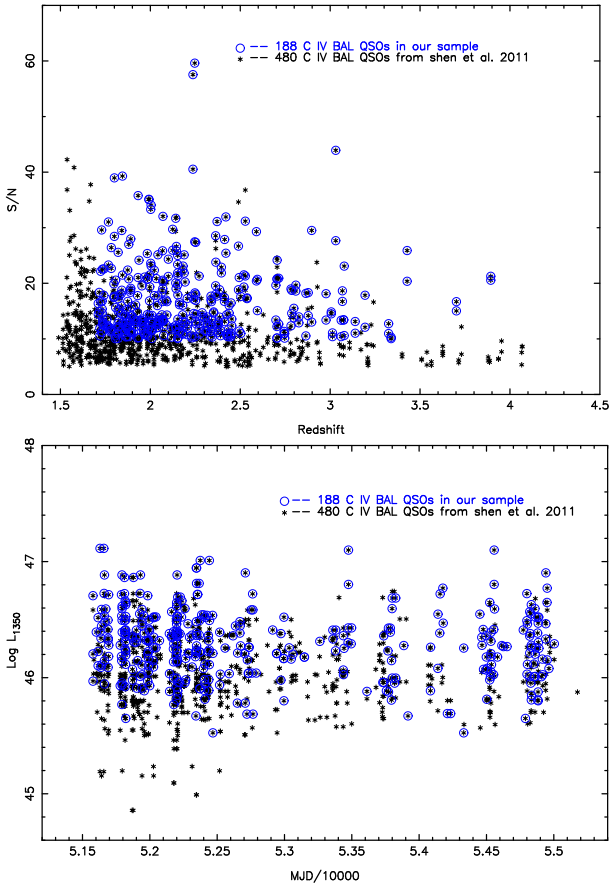

Figure 1. Top: the S/N at r-band versus the redshift. Bottom: the continuum luminosity at 1350 Å (L_{1350}, in units of erg $\mathrm{s^{-1}}$) versus the MJD. The black stars denote 480 BAL QSOs with at least two-epoch spectra from SDSS DR7. The blue circles denote 188 BAL QSOs with longest time-scale two-epoch spectra with S/N(r) $>$ 10 and z$>$1.7.

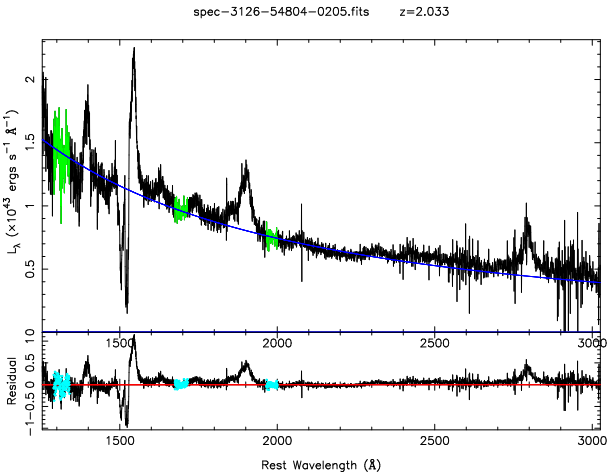

Figure 2. An example of the power-law continuum fit. Top: the extinction-corrected rest-frame spectrum is shown as the black line. The green dots are the initial continuum windows. The blue line is the power-law continuum. Bottom: the residual spectrum.

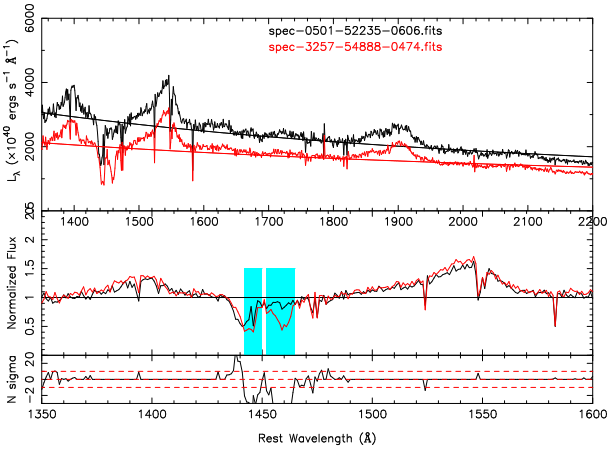

Figure 3. An example of the C IV BAL-trough variable regions. Top: two-epoch spectra as well as their continuums. Middle: their normalized spectra and the variable regions in C IV BAL troughs (cyan shaded regions). Bottom: the N_σ versus the wavelength λ. Variable regions of C IV BAL troughs are identified to be where an absorption feature is detected with $|N_\sigma| \geq 1$ for at least five consecutive data points (4 Å wide).

that by Filiz Ak et al. (2013), who used two-epoch spectra from the SDSS and the BOSS respectively.

3 SPECTRAL ANALYSIS

3.1 Fitting the spectral continuum

In order to characterize the spectral variation of BAL QSOs and the variable regions in the C IV BAL troughs, we fit the continuum spectrum by a power-law function iteratively (He et al. 2014). All the SDSS spectra are corrected for Galactic extinction, assuming the extinction curve of Cardelli et al. (1989) (IR band; UV band) and O'Donnell (1994) (optical band) with $R_V = 3.1$. The A_V values of these SDSS BAL QSOs are derived from the $SpecPhotoAll$ table in SDSS. All spectra are then corrected to the rest frame, and rebinned to a uniform grid with 1Å wide. It is popularly accepted that we can use one power-law function $f_\lambda \propto \lambda^\alpha$ ($f_\nu \propto \nu^{-(2+\alpha)}$) to fit the QSO continuum. Some authors also used two power-law functions to model the QSO continuum (e.g. Forster et al. 2001; Shang et al. 2005). For BAL QSOs, a polynomial function or a reddened power law was also used to fit the continuum in previous studies (Lundgren et al. 2007; Gibson et al. 2008, 2009). Here, we use one power-law function, $f_\lambda = f_{2000}(\lambda/2000)^\alpha$, to fit the continuum spectra of BAL QSOs (Hu et al. 2008; He et al. 2014). The power-law continuum is fit iteratively in the "continuum windows", which are known to be relatively free from strong emission lines. Our adopted continuum windows are 1290-1330, 1685-1715, 1970-2010 Å in the rest frame (Fig. 2, e.g. Forster et al. 2001; Vanden Berk et al. 2001; Gibson et al. 2008; Bian et al. 2012a; Baskin & Laor 2013). The fit is achieved by minimizing χ^2 iteratively. At each iteration, we neglect any spectral bins that deviate by more than 3σ from the previous continuum fit. This iterative method would automatically adjust the fitting window, excluding spectral regions that contain broad emission or absorption features, especially for BAL QSOs.

For the power-law continuum, $f_\lambda = f_{2000}(\lambda/2000)^\alpha$, the error of the power-law continuum by error propagation is calculated as follows (He et al. 2014):

$$\delta(f_{con}) = f_\lambda \sqrt{\left(\frac{\delta(f_{2000})}{f_{2000}}\right)^2 + (\ln\lambda - \ln 2000)^2 \delta\alpha^2}. \quad (1)$$

where the errors ($\delta(f_{2000})$ and $\delta\alpha$) are given in the power-law fitting. The total C IV BAL-trough EW is calculated as follows:

$$EW = \int [1 - \frac{f_{obv}(\lambda)}{f_{con}(\lambda)}] d\lambda. \quad (2)$$

The integration is integrated from the total C IV BAL-trough for $f_{obv}(\lambda) < f_{con}(\lambda)$. And the error for the C IV BAL EW is measured as follows:

$$\delta(EW) = \sqrt{\sum_\lambda \left(\frac{f_{obv}}{f_{con}}\right)^2 \left[\left(\frac{\delta(f_{obv})}{f_{obv}}\right)^2 + \left(\frac{\delta(f_{con})}{f_{con}}\right)^2\right]}. \quad (3)$$

where $\delta(f_{obv})$ at λ is the flux error for the SDSS spectrum.

With the continuum fit, we can obtain the spectral index α, the continuum luminosity at 1500Å, and the total C IV BAL EW, as well as their errors. These results are listed in Table 2. An example of the continuum fit and the residual is shown in Fig. 1.

3.2 Measuring the variable regions in C IV BAL troughs

In the C IV BAL tough for each QSO, it is possible to have some variable regions. To identify the variable regions in the C IV BAL-trough, we compare two-epoch spectra for BAL QSOs, measuring the flux deviation between two observations at each wavelength by the following equation (Filiz Ak et al. 2013):

$$N_\sigma(\lambda) = \frac{f_1 - f_2}{\sqrt{\sigma_1^2 + \sigma_2^2}} \quad (4)$$

where f_1 and f_2 are the normalized flux based on the fitting power-law continuum and σ_1 and σ_2 are the normalized flux error at wavelength λ. Both σ_1 and σ_2 include observational flux errors and uncertainties on the continuum model. Similar to Gibson et al. (2008), variable regions of BAL troughs are identified to be where an absorption feature is detected with $|N_\sigma| \geq 1$ for at least five consecutive data points (4 Å wide). This requirement allows detection of variable regions wider than 774 km s^{-1} . It is slightly smaller than

that by Gibson et al. (2008), and larger than that by Filiz Ak et al. (2013). For the number of data points to be lager than 5, the significance of variations would be $> 99.9\%$. 73 variable regions in the C IV BAL troughs are identified from two-epoch different spectra in 43 BAL QSOs. For the sample of 188 BAL QSOs, there are about 23% (43/188) BAL QSOs showing variable regions from two-epoch spectra. Fig. 3 gives an example of identified two variable regions in C IV BAL trough.

For each spectrum, we calculate EW and its error for each C IV BAL variable region (see above Eq. 2, Eq. 3). Then, we derive the EW variance for each C IV BAL variable region for each QSO. The sum of the EW variance for all variable regions in a QSO is adopted as its total EW variance, ΔEW. The error of ΔEW is calculated based on the error propagation from errors of EW for all variable regions. For each variable region in C IV BAL troughs, the velocity width and the center outflow velocity are also calculated, as well as the maximum outflow velocity V_{max} of variable regions. The velocity width is calculated from the left and right boundary of the variable region. In Table 3, we list the total ΔEW, the left and right boundary of the variable region for these 43 BAL QSOs.

4 RESULTS AND DISCUSSION

4.1 Features of the variable regions: velocity width, outflow velocity, variation proportion

With the above criterion of at least five consecutive data points larger than 1σ, 73 variable regions in the C IV BAL troughs are identified from 43 two-epoch different spectra. Fig. 4 shows histograms of their velocity width and their center outflow velocity (Table 3). BAL-troughs variation tends to occur on small velocity width. Even the largest variation widths (6500 km s^{-1}) are narrow compared to BAL-trough outflow velocity (bottom panel of Fig. 4). The number of the C IV BAL variable regions decreases with the increase of the velocity width of the variable regions. These results are consistent with that by Gibson et al. (2008).

From the bottom panel of Fig. 4, variable regions are found across a wide range of central outflow velocities, and the number of variable regions appears to peak in the range between 5000 and 21000 km s^{-1} . Considering BI_0 used by Shen et al. (2011), $0\,\mathrm{km\,s^{-1}}$ is adopted as a minimum detection limit for BAL-trough. We do not consider contaminations from C IV 1549, Si IV 1399 emission lines at small outflow velocities and large outflow velocities, respectively. It could explain decrease of number of variable regions at small outflow velocities and at large outflow velocities in the bottom panel in Fig. 4.

In Fig. 5, we give the distribution of the time-interval between epochs for total 188 BAL QSOs (top panel), as well as the time-interval histogram for 43 BAL QSOs showing variable regions (middle panel). It covers a time-interval of about 0.001 – 3 years in the rest frame. The bottom panel in Fig. 5 is the number ratio of the middle panel to the top panel, i.e., the proportion of BAL QSOs showing variable regions versus the time-interval. It is clear that the proportion of BAL QSOs showing variable regions increases with the time-interval, rising to 50% when the time-interval is longer than about 1 year in the rest frame. This result gives a good reason to consider only the longest time-interval spectral pairs for each QSO. Larger proportion of BAL trough showing variable region across longer time-interval is consistent with the result by Capellupo et al. (2013).

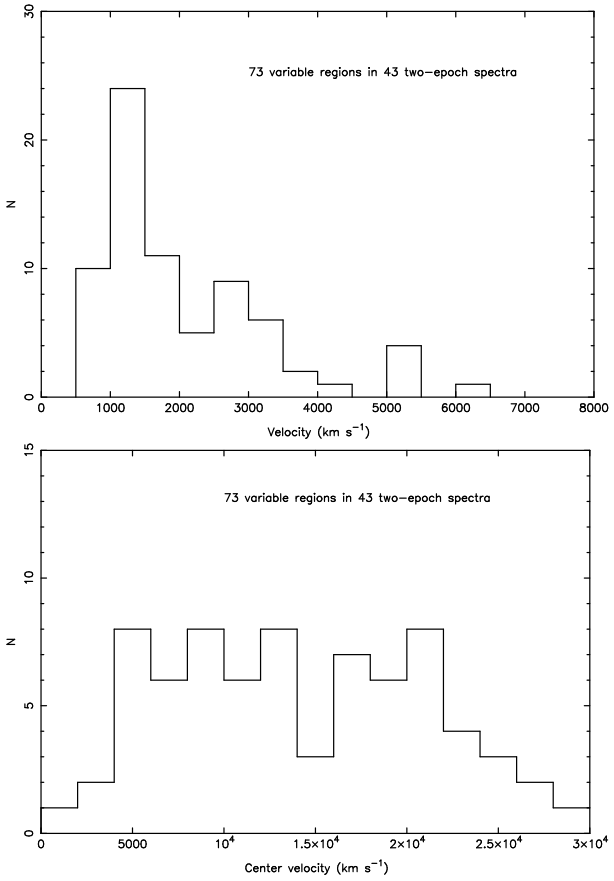

Figure 4. Histograms for the 73 identified variable C IV BAL regions. Top: the distribution of the velocity width of the variable regions. Bottom: the distribution of the center outflow velocity of the variable regions.

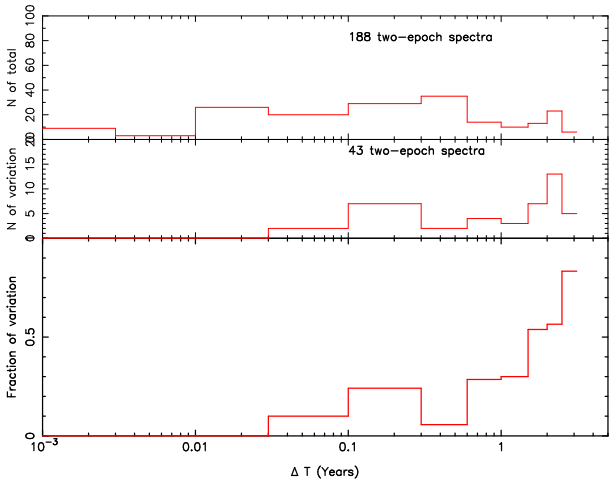

Figure 5. Top: distribution of the time-interval between two epochs for all 188 BAL QSOs. Middle: distribution of the time-interval between two epochs for 43 C IV BAL QSOs with variable regions. Bottom: the number ratio of the middle panel to the top panel. The time-interval is in the rest frame of BAL QSOs.

Table 1. Summary of the Spearman correlation coefficients: For total sample of 188 BAL QSOs, ΔEW is the BAL-trough EW variation from two-epoch spectra, and there are 116 BAL QSOs with available Mg II -based $M_{\rm BH}$. For 43 BAL QSOs with variable regions, ΔEW is the EW variation of the C IV BAL-trough variable regions, and there are 28 BAL QSOs with available Mg II -based $M_{\rm BH}$. ΔL_{1500} is the variation of the continuum at 1500 Å. $\Delta\alpha$ is the variation of the spectral index. $M_{\rm BH}$ is the Mg II -based SMBH masses from a single spectrum. L_{bol}/L_{Edd} is the ratio of the bolometric luminosity to the Eddington luminosity. V_{max} is the maximum velocity of the variable region. The value in brackets is the probability of the null hypothesis.

	$\Delta L_{1500}-\Delta\alpha$	$\Delta EW-\Delta\alpha$	$\Delta EW-\Delta L_{1500}$	$\Delta EW-M_{BH}$	$V_{max}-L_{bol}/L_{Edd}$
Total sample	$-0.36(5.5E-07)$	$-0.008(0.91)$	-0.17 (0.02)	-0.15(0.1)	-
Subsample	$-0.56(8.3E-05)$	$0.30(0.05)$	-0.44 (0.003)	-0.54(0.003)	0.53 (0.004)

4.2 The variability of spectral index $\Delta\alpha$ for BAL QSOs with variable regions

It has been shown that QSOs spectra are bluer during their brighter phases. It is usually explained by the variation of the accretion disk. Fig. 6 shows $\Delta\alpha$ versus the continuum variation at 1500Å (ΔL_{1500}) for total 188 BAL QSOs (the top panel). There is a significant weak correlation between them. The Spearman coefficient R is -0.36, with the the probability of the null hypothesis of $P_{\rm null}=5.5\times10^{-7}$ (see Table 1). In the second and fourth quadrants in the top panel in Fig. 6, BAL QSOs show bluer during their brighter phase. There are about 56.9% date points showing bluer during their brighter phase. It is consistent with the result for non-BAL QSOs by Bian et al. (2012a). Considering 11 points with both ΔL_{1500} and $\Delta\alpha$ more than 3σ, the proportion rises to 84.6% (11/13), more QSOs appear bluer during their brighter phases compared to non-BAL QSOs (the bottom panel in Fig. 6).

For the subsample of BAL QSOs with variable regions in C IV BAL troughs, there is a significant medium strong correlation between the ΔL_{1500} and $\Delta\alpha$. The Spearman coefficient R is -0.56, $P_{\rm null}=8.3\times10^{-5}$ (see Table 1). There are about 76.7% BAL QSOs showing bluer during their brighter phases for 43 BAL QSOs (red circles in the top panel in Fig. 6). Considering 6 BAL QSOs with both ΔL_{1500} and $\Delta\alpha$ more than 3σ, the proportion of the points in the second and fourth quadrants rises to 100% (6/6) (red circles in bottom panel in Fig. 6).

The proportion showing bluer during the brighter phases rises from about 56.9% for total 188 BAL QSOs to about 76.7% for 43 BAL QSOs with variable regions. During the brighter phases, the accretion disk becomes hotter and its emission peak would move to shorter wavelengths. It may lead to the trend of bluer spectra during brighter phases. Therefore, this larger proportion implies that the origin of variable BAL-trough regions is related to the central accretion process.

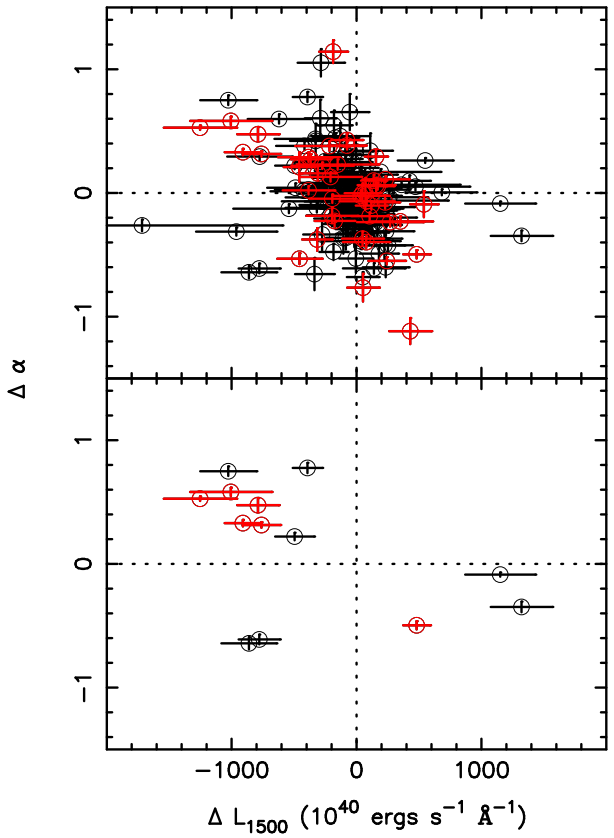

Figure 6. $\Delta\alpha$ versus ΔL_{1500} for 188 BAL QSOs (top), and for 13 BAL QSOs with both ΔL_{1500} and $\Delta\alpha$ more than 3σ (bottom). The proportion of the points in the second and fourth quadrants (i.e., bluer during brighter phases) rises from about 56.9% (top) to 84.6% (bottom). The red circles denote 43 BAL QSOs with variable regions (top), and 6 QSOs with both ΔL_{1500} and $\Delta\alpha$ more than 3σ (bottom). The proportion of the points in the second and fourth quadrants is 76.7%. For 6 QSOs with both ΔL_{1500} and $\Delta\alpha$ more than 3σ, the proportion of the points in the second and fourth quadrants rises to 100%.

4.3 The EW variability ΔEW for the variable region: the relation with $\Delta\alpha$, ΔL_{1500}

For the subsample of 43 BAL QSOs with variable regions in C IV BAL troughs, the relation between ΔEW and $\Delta\alpha$, ΔL_{1500} are used to investigate the origin of BAL variability (see Table 2, Table 3). Fig. 7 shows ΔEW versus $\Delta\alpha$ (top panel). It is possible that there is a weak correlation between ΔEW and $\Delta\alpha$, according to a Spearman rank correlation test ($R=0.3$, $P_{\rm null}=0.05$; Table 1). There are 60.5% of QSOs located in the first and third quadrants where the BAL-troughs become stronger when BAL QSOs become redder. This is different from our previous study for a single BAL QSOs with 18 epochs (He et al. 2014). He et al. (2014) found a strong correlation between EW variation for C IV BAL-trough and $\Delta\alpha$ (R=0.77), suggesting that dust is intrinsic to outflows. For the subsample of BAL QSOs with variable regions, we don't confirm that strong correlation from the two-epoch variation. It is possibly due to the additional parameters to blur this correlation. For the total sample of 188 BAL QSOs, there is no correlation between ΔEW and $\Delta\alpha$, where ΔEW is the EW variation for C IV BAL-trough. A Spearman rank correlation test gives $R=-0.008$, $P_{\rm null}=0.91$ (Table 1).

The bottom panel in Fig. 7 shows ΔEW versus ΔL_{1500} for 43 BAL QSOs with variable regions. It is possible that there is a medium strong correlation between them, $R=-0.44, P_{\rm null}=0.003$ (Table 1). It is found that 60.5% QSOs located in the second and fourth quadrants, where BAL troughs become weaker

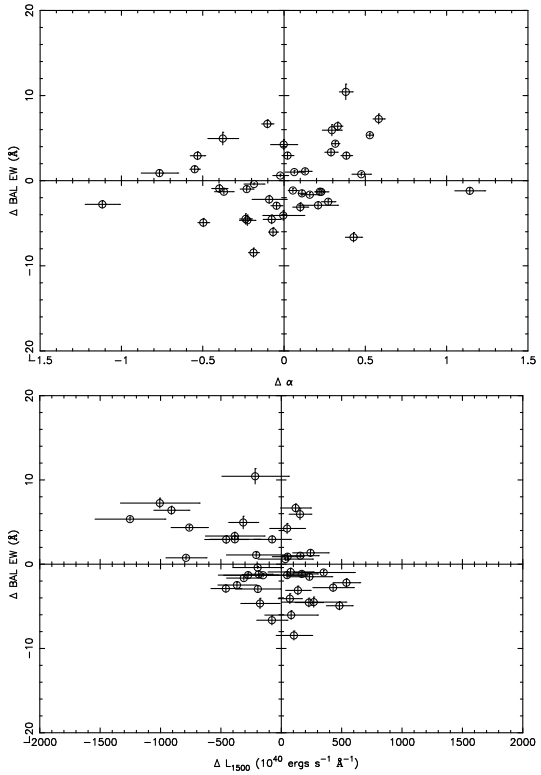

Figure 7. Top: ΔEW versus $\Delta\alpha$ for 43 epochs in BAL QSOs with variable regions. The Spearman correlation coefficient R is 0.3 with $P_{\rm null} = 0.05$. Bottom: ΔEW versus ΔL_{5100} for 43 epochs in BAL QSOs with variable regions, $R = -0.44$, $P_{\rm null} = 0.003$.

when BAL QSOs become brighter. For the total sample of 188 BAL QSOs, ΔEW is the EW variation for C IV BAL-trough, and $R = -0.17, P_{\rm null} = 0.02$ (Table 1). Therefore, we don't find a significant correlation between them. It is consistent with the study of Filiz Ak et al. (2013), who found no significant evidence for EW variability of the C IV BAL trough driven by QSO bolometric luminosity (also see Gibson et al. 2008). With respect to total sample of 188 BAL QSOs, the subsample of 43 BAL QSOs with variable regions has a stronger correlation between them. Considering the probability of the null hypothesis ($P_{\rm null} = 0.003$) for the subsample of 43 BAL QSOs with variable regions, this correlation is suggestive and requires further investigations by larger sample.

4.4 The relation of ΔEW with the central accretion properties, $M_{\rm BH}$, $L_{\rm bol}/L_{\rm Edd}$

The relation between the BAL properties/variability and the accretion process in BAL QSOs has been discussed by many authors (e.g. Laor & Brandt 2002; Ganguly et al. 2007; Baskin & Laor 2013; Filiz Ak et al. 2013; He et al. 2014). There are two fundamental parameters related to the accretion process, the SMBH mass ($M_{\rm BH}$) and the Eddington ratio ($L_{\rm bol}/L_{\rm Edd}$). Considering that the C IV -based SMBH mass is biased to the possible non-virialized component in C IV emission lines (e.g. Rafiee & Hall 2011; Shen et al. 2011; Bian et al. 2012b), we used Mg II -based $M_{\rm BH}$ to investigate the relation of ΔEW with the central accretion properties, such as $M_{\rm BH}$, and $L_{\rm bol}/L_{\rm Edd}$. Fitting Mg II 2800 emission lines, Shen et al. (2011) gave the Mg II -based $M_{\rm BH}$ for QSOs with $0.35 \leq z \leq 2.25$. For the subsample of BAL QSOs with variable regions in C IV BAL toughs, there are 28 BAL QSOs with measured Mg II -based $M_{\rm BH}$ by Shen et al. (2011). The bolometric luminosity ($L_{\rm bol}$) is calculated from L_{3000} ($0.7 \leq z \leq 1.9$), L_{1350} ($z \geq 1.9$). With the bolometric corrections (BC) from the luminosity at 3000 Å and 1350 Å as $BC_{3000} = 5.15$, $BC_{1350} = 3.81$, we calculate $L_{\rm bol}/L_{\rm Edd}$. These results are listed in Table 3.

In Fig. 8, we show the relation between $|\Delta EW|$ and Mg II -based $M_{\rm BH}$. It is possible that there is a negative medium strong correlation between the $|\Delta EW|$ and $M_{\rm BH}$ ($R = -0.54, P_{null} = 0.003$, Table 1), showing smaller variation of BAL-trough for BAL QSOs with larger SMBHs masses. In Fig. 9, we shows the relation between the maximum outflow velocity of variable regions (V_{max}) and the Eddington ratio $L_{\rm bol}/L_{\rm Edd}$. It is possible that there is a medium strong correlation between the V_{max} and $L_{\rm bol}/L_{\rm Edd}$ ($R = 0.53, P_{null} = 0.004$, Table 1), showing larger outflow velocity for BAL QSOs with larger Eddington ratio. Considering the test confidence less than 99.9% for the subsample of 43 BAL QSOs, these correlations are suggestive. For the total 188 BAL QSOs, there are 116 BAL QSOs with available Mg II -based $M_{\rm BH}$, and there is no significant correlation between $|\Delta EW|$ and $M_{\rm BH}$ ($R = -0.15, P_{null} = 0.1$, Table 1).

In Figs. 8, 9, there is an outlier, SDSS J020006.31-003709.7 ($z = 2.141$), with largest $M_{\rm BH}$ and smallest $L_{\rm bol}/L_{\rm Edd}$ in Table 3. Excluding this QSO, these correlations would be stronger and significant. For the relation between $|\Delta EW|$ and $M_{\rm BH}$, $R = -0.7, P_{null} = 0.00005$. For the relation between V_{max} and $L_{\rm bol}/L_{\rm Edd}$, $R = 0.58, P_{null} = 0.0014$. These results imply the connection between the BAL-trough variation and the central accretion process. Using C IV -based SMBH mass for BAL QSOs ($z > 2$), Filiz Ak et al. (2013) suggested possible correlations between $|\Delta EW|$ and luminosity/Eddington ratio for C IV troughs on moderate time-scales (1-2.5 yrs). They did not find significant correlation between $|\Delta EW|$ and $M_{\rm BH}$. These correlations require further investigations in larger samples of BAL QSOs with no bias $M_{\rm BH}$ estimation such as from Hβ , Mg II emission lines.

We don't find a significant correlation between V_{max} and α, $L_{\rm bol}$. We don't confirm the result by Laor & Brandt (2002), who found that V_{max} increase with $L_{\rm bol}$. We find that $L_{\rm bol}/L_{\rm Edd}$ instead of $L_{\rm bol}$ is a driver of V_{max} . In the future, we can use the BOSS spectra to estimate the $M_{\rm BH}$ because of their larger wavelength coverage in BOSS spectra than in SDSS spectra.

5 SUMMARY

The variability of broad absorption lines is investigated for a sample of 188 BAL QSOs ($z > 1.7$) with at least two-epoch observations from the SDSS DR7. Considering only the longest time-scale between epochs for each QSO, 73 variable regions in the C IV BAL troughs are detected for 43 BAL QSOs. The main conclusions can be summarized as follows.

(1) Considering the flux deviation $|N_\sigma| \geq 1$ for at least five consecutive data points (4 Å wide) in the two-epoch difference spectrum, 73 C IV BAL variable regions in 43 BAL QSOs are identified from 188 BAL QSOs, i.e., about 23% (43/188) BAL QSOs showing variable regions from two-epoch spectra. It is found that the proportion of BAL QSOs showing variable regions increases with the time-interval longer than about 1 year in the rest frame. BAL variation tends to occur on small velocity width. Even the largest variation widths (6500 km s^{-1}) are narrow compared to BAL-trough outflow velocity. Variable regions are found across a

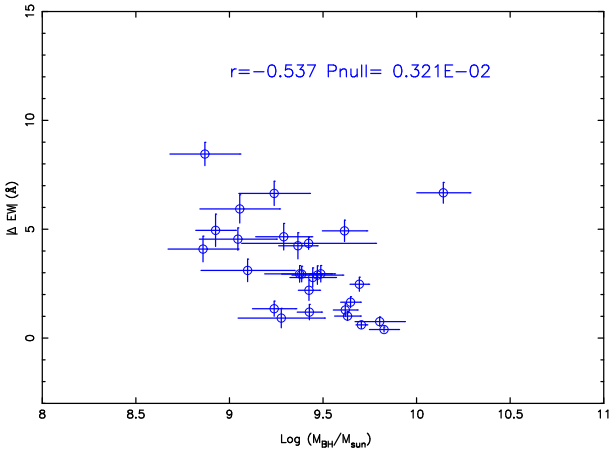

Figure 8. $|\Delta EW|$ versus the Mg II -based $M_{\rm BH}$ for 28 BAL QSOs with variable regions. The Spearman correlation coefficient R is -0.54 with $P_{null} = 0.003$.

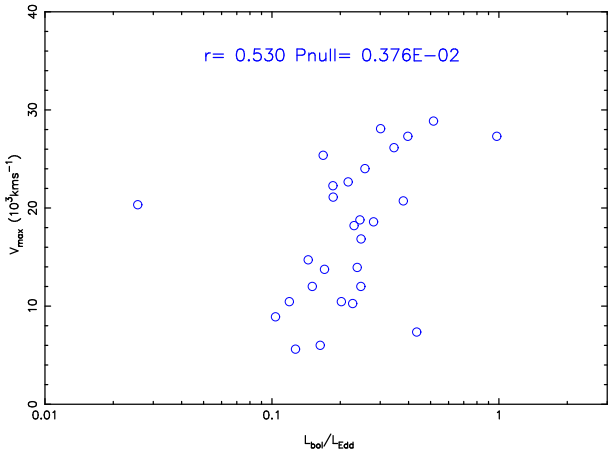

Figure 9. The maximum outflow velocity of variable regions (V_{max}) versus the Eddington ratio $L_{\rm bol}/L_{\rm Edd}$ for 28 BAL QSOs with variable regions. The Spearman correlation coefficient R is 0.53 with $P_{null} = 0.004$.

wide range of outflow velocities, and the number of variable regions appears to peak in the range between $\sim$ 5000 and $\sim$ 21000 km s^{-1} .

(2) With two-epoch variation, it is found that there is a weak correlation between ΔL_{1500} and $\Delta\alpha$ for total 188 two-epoch spectra, and about half BAL QSOs appear redder during their brighter phases. It is consistent with the result for non-BAL QSOs by (Bian et al. 2012a). For a subsample of BAL QSOs with variable regions in BAL toughs, their correlation becomes stronger, about 76.7% BAL QSOs appear bluer during their brighter phases. This larger proportion implies that the origin of variable regions in BAL-trough is related to the central accretion process.

(3) For the subsample of 43 BAL QSOs with variable regions, it is possible that there is a weak correlation between ΔEW and $\Delta\alpha$. It is different from our previous study for a single BAL QSOs by (He et al. 2014). It is possibly due to the additional parameters to blur this correlation. It is possible that there is a medium strong correlation between ΔEW and ΔL_{5100}. Considering the test confidence is 99.7%, this latter correlation is suggestive and requires further investigations by larger sample.

(4) For the subsample of 43 BAL QSOs with variable regions, there are 28 BAL QSOs with available Mg II -based $M_{\rm BH}$. It is possible that there is a negative medium strong correlation between the $|\Delta EW|$ and $M_{\rm BH}$, showing smaller variation of BAL-trough for BAL QSOs with larger SMBHs masses. It is possible that there is a medium strong correlation between V_{max} of variable regions and $L_{\rm bol}/L_{\rm Edd}$, showing larger outflow velocity for BAL QSOs with larger Eddington ratio. These results imply the connection between the BAL-trough variation and the central accretion process. These correlations require further investigations in larger samples of BAL QSOs with no bias $M_{\rm BH}$ estimation such as from Hβ , Mg II emission lines.

6 ACKNOWLEDGMENTS

We are very grateful to the anonymous referee for her/his instructive comments which significantly improved the content of the paper. This work has been supported by the National Science Foundations of China (Nos. 11373024, 11173016 and 11233003).

REFERENCES

Allen J. T., et al. 2011, MNRAS, 410, 860
Baskin A., Laor A., & Hamann F. 2013, MNRAS, 432, 1525
Bentz M. C., Peterson B. M., Netzer H., Pogge R. W., & Vestergaard M. 2009, ApJ, 697, 160
Bian W. H., et al., 2012a, ApJ, 759, 88
Bian W. H., et al., 2012b, MNRAS, 427, 2881
Bruni G., et al., 2012, A&A, 542, 13
Capellupo D. M., et al., 2011, MNRAS, 413, 908
Capellupo D. M., et al., 2012, MNRAS, 422, 3249
Capellupo D. M., et al., 2013, MNRAS, 429, 1872
Cardelli J. A., Clayton G. C., & Mathis J. S., 1989, ApJ, 345, 245
Elvis M., 2000, ApJ, 545, 63
Fabian A. C., 2012, ARA&A, 50, 455
Filiz Ak, N., er al., 2012, ApJ, 757, 114
Filiz Ak, N., er al., 2013, ApJ, 777, 168
Fine S., Jarvis M.J., & Mauch T., 2011, MNRAS, 412, 213
Forster K., et al., 2001, ApJS, 134, 35
Ganguly R., Brotherton M. S., Cales S., et al. 2007, ApJ, 665, 990
Gibson R. R., et al., 2008, ApJ, 675, 985
Gibson R. R., et al., 2009, ApJ, 692, 758
Grier C. J., et al., 2015, ApJ, 806, 111
Guo H. X., & Gu M. F., 2014, JApA, 35, 477
Hewett P. C., & Foltz, C. B., Chaffee, F. H., 1995, AJ, 109, 1498H
He Z. C., Bian W. H., Jiang X. L., & Wang Y. F., 2014, MNRAS, 443, 2532
Hu C., Wang J. M., Ho L. C., Chen Y. M., Zhang H. T., Bian, W. H., Xue, S. J., 2008, ApJ, 687, 78
Kaspi S., Maoz D., Netzer H., et al. 2005, ApJ, 629, 61
Laor A., & Brandt W. N., 2002, ApJ, 569, 64
Lundgren B. F., Wilhite B. C., Brunner R. J., et al., 2007, ApJ, 656, 73
Margala D, et al., ApJ, arXiv:1506.04790v1
Meusinger H., Hinze, A., de Hoon, A., 2011, A&A, 525, 37
Montenegro-Montes F. M., et al.,2008, MNRAS, 388, 1853
Murray N., Chiang J., Grossman S. A., & Voit G. M., 1995, ApJ, 451, 498
O'Donnell J. E., 1994, ApJ, 422, 158
Paris I. et al., 2014, A&A, 563, 54
Proga D., Stone J. M., & Kallman T. R., 2000, ApJ, 543, 686

Pu X. T., Bian W. H., & Huang K. L., 2006, MNRAS, 372, 24
Rafiee A., & Hall P. B., 2011, MNRAS, 415, 2932
Shang Z. H., et al., 2005, ApJ, 619, 41
Shen Y., et al., 2011, ApJS, 194, 45
Trump J. R., et al., 2006, ApJS, 165, 1
Urry C. M., & Padovani P., 1995, PASP, 107, 803
Vanden Berk D. E., Richards G. T., Bauer A., et al., 2001, AJ, 122, 54
Weymann R. J., Morris S. L., Foltz C. B., & Hewett P. C., 1991, ApJ, 373, 23
Wilhite, B. C., et al., 2005, ApJ, 633, 638
York D. G., Adelman J., Anderson J. E., et al. 2000, AJ, 120, 1579
Zubovas K., & King, A., 2013, ApJ, 769, 51
Zuo W. W., et al., 2012, ApJ, 758, 104

Table 2. The properties of 188 BAL QSOs. Col. (1) is the No. of BAL QSOs. Col. (2) is No. of the epoch. Col. (3) is the SDSS name. Col. (4) is the redshift. Col. (5) is Plate-MJD-Fiber of the observation. Col. (6) is luminosity in units of $10^{40}\mathrm{erg\,s^{-1}}\mathring{A}^{-1}$. Col. (7) is the UV spectral index. Col. (8) is the total C IV BAL EW in units of Å.

No. (1)	epoch (2)	name (3)	z (4)	Plate-MJD-Fiber (5)	L_{1500} (6)	α (7)	BAL EW (8)
001	01	J001130.55+005550.7	2.309	0389-51795-0339	1860.73 ± 220.18	-1.18 ± 0.04	12.03 ± 1.21
001	02	J001130.55+005550.7	2.309	0686-52519-0603	1475.93 ± 154.57	-1.15 ± 0.03	10.18 ± 1.10
002	01	J001438.28-010750.1	1.806	0389-51795-0211	770.10 ± 148.78	-0.88 ± 0.13	24.11 ± 2.07
002	02	J001438.28-010750.1	1.806	0687-52518-0249	615.19 ± 128.45	-0.81 ± 0.13	21.59 ± 2.29
003	01	J002127.88+010420.1	1.820	0390-51816-0445	1604.75 ± 143.90	-1.75 ± 0.08	14.41 ± 0.98
003	02	J002127.88+010420.1	1.820	0688-52203-0374	1349.17 ± 129.10	-1.70 ± 0.08	14.40 ± 1.04
004	01	J002146.71-004847.9	2.503	0390-51816-0161	1824.74 ± 183.96	-1.22 ± 0.04	5.35 ± 1.10
004	02	J002146.71-004847.9	2.503	0390-51900-0180	2074.63 ± 134.06	-1.42 ± 0.02	4.82 ± 0.69
005	01	J002710.06-094435.3	2.070	0653-52145-0556	1869.96 ± 126.53	-0.76 ± 0.03	16.80 ± 0.75
005	02	J002710.06-094435.3	2.070	3105-54825-0310	1974.66 ± 75.48	-0.95 ± 0.01	10.82 ± 0.41
006	01	J003312.25+155442.4	1.937	0417-51821-0576	770.90 ± 88.62	-1.20 ± 0.12	69.25 ± 1.26
006	02	J003312.25+155442.4	1.937	3133-54789-0379	841.70 ± 38.27	-1.21 ± 0.05	62.26 ± 0.51
007	01	J004118.59+001742.4	1.765	0392-51793-0631	723.13 ± 113.58	-1.05 ± 0.10	16.72 ± 1.55
007	02	J004118.59+001742.4	1.765	0690-52261-0553	712.34 ± 91.32	-1.38 ± 0.10	13.40 ± 1.41
008	01	J004323.43-001552.4	2.798	0393-51794-0181	3052.29 ± 367.63	-0.86 ± 0.02	9.68 ± 1.03
008	02	J004323.43-001552.4	2.798	0690-52261-0028	2511.14 ± 252.10	-0.99 ± 0.03	12.28 ± 1.17
009	01	J004527.68+143816.1	1.992	0419-51812-0105	3911.52 ± 164.76	-0.27 ± 0.03	27.37 ± 0.52
009	02	J004527.68+143816.1	1.992	0419-51868-0106	3944.77 ± 154.36	-0.30 ± 0.03	28.71 ± 0.48
010	01	J004613.54+010425.7	2.152	0393-51794-0572	2955.44 ± 172.22	-1.66 ± 0.02	39.71 ± 0.54
010	02	J004613.54+010425.7	2.152	0691-52199-0460	2858.19 ± 131.32	-1.67 ± 0.02	37.86 ± 0.42
011	01	J004732.73+002111.3	2.878	0393-51794-0588	2669.00 ± 276.06	-1.91 ± 0.03	8.81 ± 1.12
011	02	J004732.73+002111.3	2.878	0691-52199-0559	2749.06 ± 207.40	-1.89 ± 0.02	8.81 ± 0.83
012	01	J004806.05-010321.6	2.528	0394-51812-0299	3502.07 ± 173.05	-1.73 ± 0.02	4.79 ± 0.55
012	02	J004806.05-010321.6	2.528	3111-54800-0281	4051.75 ± 136.42	-1.47 ± 0.01	3.70 ± 0.37
013	01	J005419.99+002727.9	2.490	0394-51812-0511	2561.01 ± 152.81	-1.13 ± 0.02	16.86 ± 0.62
013	02	J005419.99+002727.9	2.490	3111-54800-0509	2793.79 ± 106.36	-1.02 ± 0.01	13.95 ± 0.39
014	01	J010859.53-105757.8	1.807	0659-52199-0099	1260.76 ± 105.13	-1.18 ± 0.07	48.50 ± 1.02
014	02	J010859.53-105757.8	1.807	3109-54833-0003	945.67 ± 58.56	-1.56 ± 0.06	52.70 ± 0.72
015	01	J010920.96-100127.0	2.449	2864-54467-0320	1277.23 ± 72.02	-1.68 ± 0.02	9.86 ± 0.63
015	02	J010920.96-100127.0	2.449	3109-54833-0080	884.09 ± 93.49	-0.91 ± 0.04	9.54 ± 1.17
016	01	J012603.62-100114.8	2.302	0661-52163-0114	1512.19 ± 160.55	-1.95 ± 0.03	22.54 ± 1.06
016	02	J012603.62-100114.8	2.302	2878-54465-0274	1055.95 ± 77.02	-2.48 ± 0.03	31.04 ± 0.79
017	01	J013012.36+153158.0	2.352	0425-51898-0445	1778.04 ± 174.69	0.07 ± 0.03	20.49 ± 1.06
017	02	J013012.36+153158.0	2.352	0425-51884-0446	1769.05 ± 189.22	-0.18 ± 0.04	23.50 ± 1.15
018	01	J013038.79+391818.1	2.520	2062-53381-0623	2139.81 ± 119.40	-1.27 ± 0.02	13.34 ± 0.60
018	02	J013038.79+391818.1	2.520	2063-53359-0024	2024.22 ± 121.10	-1.39 ± 0.02	12.69 ± 0.64
019	01	J013625.65-103346.2	2.009	0662-52147-0002	799.65 ± 121.52	-0.14 ± 0.08	42.02 ± 1.68
019	02	J013625.65-103346.2	2.009	1915-53612-0133	650.34 ± 75.17	-0.27 ± 0.05	42.34 ± 1.26
020	01	J013656.31-004623.7	1.716	0400-51820-0003	1338.49 ± 183.80	-1.10 ± 0.09	13.55 ± 1.52
020	02	J013656.31-004623.7	1.716	0698-52203-0202	1158.39 ± 124.19	-0.83 ± 0.06	19.78 ± 1.15
021	01	J014948.74+141300.9	2.188	0429-51820-0584	1745.76 ± 104.38	-1.43 ± 0.02	7.85 ± 0.62
021	02	J014948.74+141300.9	2.188	1899-53262-0548	1740.28 ± 82.23	-1.53 ± 0.02	7.84 ± 0.51
022	01	J015048.83+004126.2	3.702	0402-51793-0505	5558.73 ± 320.86	-1.30 ± 0.04	10.18 ± 0.63
022	02	J015048.83+004126.2	3.702	0699-52202-0629	5319.60 ± 315.36	-1.29 ± 0.05	12.07 ± 0.68
023	01	J020006.31-003709.7	2.141	0403-51871-0070	1846.41 ± 112.19	-0.41 ± 0.03	40.36 ± 0.73
023	02	J020006.31-003709.7	2.141	2866-54478-0197	1964.77 ± 54.49	-0.51 ± 0.02	48.21 ± 0.39
024	01	J021818.14-092153.5	1.880	0668-52162-0218	2259.30 ± 149.56	-1.62 ± 0.05	16.67 ± 0.73
024	02	J021818.14-092153.5	1.880	3122-54821-0201	1470.26 ± 73.36	-1.14 ± 0.03	19.90 ± 0.51
025	01	J022036.27-081242.9	2.004	0668-52162-0547	2005.37 ± 129.03	-0.89 ± 0.03	20.99 ± 0.71
025	02	J022036.27-081242.9	2.004	3122-54821-0482	2247.01 ± 71.30	-1.44 ± 0.01	20.66 ± 0.36
026	01	J022349.24+004727.8	2.335	0704-52205-0459	912.86 ± 100.24	-1.24 ± 0.09	13.93 ± 1.19
026	02	J022349.24+004727.8	2.335	3127-54835-0338	964.99 ± 77.56	-2.01 ± 0.07	19.04 ± 0.82
027	01	J022844.09+000217.0	2.705	0406-51817-0035	3900.33 ± 187.14	-1.02 ± 0.02	18.87 ± 0.70
027	02	J022844.09+000217.0	2.705	0406-52238-0039	3854.36 ± 202.67	-0.94 ± 0.02	22.61 ± 0.73
028	01	J023139.53+001758.4	2.375	0407-51820-0483	1583.17 ± 118.98	-1.82 ± 0.03	9.29 ± 0.87
028	02	J023139.53+001758.4	2.375	0705-52200-0505	1372.57 ± 107.43	-1.82 ± 0.03	12.73 ± 0.94
029	01	J023252.80-001351.1	2.033	0705-52200-0063	1231.68 ± 111.34	-1.95 ± 0.04	26.64 ± 1.08
029	02	J023252.80-001351.1	2.033	3126-54804-0205	1153.97 ± 57.90	-1.53 ± 0.02	17.54 ± 0.58
030	01	J023820.90+001419.7	2.782	0706-52199-0472	2195.28 ± 223.61	-1.94 ± 0.03	22.57 ± 1.28
030	02	J023820.90+001419.7	2.782	3126-54804-0500	1878.07 ± 115.63	-2.06 ± 0.02	18.17 ± 0.72

Table 2. – continue

No. (1)	epoch (2)	name (3)	z (4)	Plate-MJD-Fiber (5)	L_{1500} (6)	α (7)	BAL EW (8)
031	01	J023903.43-003850.8	3.075	0408-51821-0134	2955.93 ± 219.75	-1.50 ± 0.03	6.99 ± 0.98
031	02	J023903.43-003850.8	3.075	0706-52199-0179	2807.41 ± 207.90	-1.61 ± 0.03	7.91 ± 0.92
032	01	J024221.87+004912.6	2.069	0408-51821-0576	2171.53 ± 137.44	-1.00 ± 0.02	19.70 ± 0.63
032	02	J024221.87+004912.6	2.069	0706-52199-0617	2028.23 ± 147.32	-0.98 ± 0.03	21.83 ± 0.71
033	01	J024224.02+010452.5	2.433	0408-51821-0564	1394.86 ± 152.27	-0.61 ± 0.04	12.18 ± 1.16
033	02	J024224.02+010452.5	2.433	0706-52199-0606	1065.54 ± 137.63	-0.41 ± 0.04	11.56 ± 1.37
034	01	J024304.68+000005.4	1.995	0408-51821-0080	1674.30 ± 135.82	-1.60 ± 0.03	13.76 ± 0.83
034	02	J024304.68+000005.4	1.995	0706-52199-0080	1464.74 ± 133.02	-1.78 ± 0.04	14.05 ± 1.00
035	01	J024701.18+000330.2	2.152	0409-51871-0472	745.43 ± 118.16	0.11 ± 0.06	8.28 ± 1.62
035	02	J024701.18+000330.2	2.152	1664-52973-0474	659.55 ± 48.46	0.21 ± 0.03	6.50 ± 0.79
036	01	J025042.45+003536.7	2.385	0410-51816-0352	1730.23 ± 157.63	-0.49 ± 0.03	40.90 ± 1.02
036	02	J025042.45+003536.7	2.385	1664-52973-0548	951.55 ± 50.05	-1.10 ± 0.02	43.20 ± 0.58
037	01	J025331.93+001624.6	1.821	0410-51816-0391	1174.54 ± 155.96	-2.00 ± 0.10	9.37 ± 1.44
037	02	J025331.93+001624.6	1.821	0708-52175-0472	1130.18 ± 95.74	-2.01 ± 0.07	5.25 ± 0.95
038	01	J031331.22-070422.8	2.786	0459-51924-0490	2468.98 ± 220.86	-1.85 ± 0.03	41.52 ± 1.03
038	02	J031331.22-070422.8	2.786	3185-54829-0623	1848.56 ± 120.53	-1.25 ± 0.02	42.18 ± 0.73
039	01	J031609.83+004043.1	2.897	0413-51821-0386	3229.25 ± 401.19	-1.16 ± 0.03	9.04 ± 1.19
039	02	J031609.83+004043.1	2.897	3183-54833-0465	3258.12 ± 164.31	-1.28 ± 0.01	8.83 ± 0.46
040	01	J031828.90-001523.1	1.985	0413-51821-0166	3089.15 ± 166.78	-1.82 ± 0.02	7.94 ± 0.59
040	02	J031828.90-001523.1	1.985	0711-52202-0114	2600.48 ± 154.31	-1.78 ± 0.03	10.64 ± 0.65
041	01	J032118.22-010539.9	2.412	0413-51821-0055	2625.51 ± 193.52	-0.12 ± 0.03	23.14 ± 0.85
041	02	J032118.22-010539.9	2.412	0712-52199-0287	1598.91 ± 115.59	0.63 ± 0.03	18.29 ± 0.87
042	01	J032701.43-002207.1	2.319	0414-51869-0152	1666.84 ± 151.69	-1.43 ± 0.03	12.03 ± 0.90
042	02	J032701.43-002207.1	2.319	0712-52199-0159	1727.30 ± 179.78	-1.60 ± 0.03	11.20 ± 1.00
043	01	J033029.75-005918.1	2.747	0414-51869-0004	1860.40 ± 228.82	-1.23 ± 0.04	9.48 ± 1.55
043	02	J033029.75-005918.1	2.747	0414-51901-0021	1654.68 ± 195.10	-0.98 ± 0.04	20.70 ± 1.62
044	01	J074123.74+190453.8	2.288	2074-53437-0325	866.49 ± 71.04	-1.08 ± 0.03	7.66 ± 0.86
044	02	J074123.74+190453.8	2.288	2915-54497-0338	852.48 ± 73.87	-1.08 ± 0.03	11.03 ± 0.90
045	01	J074221.38+165740.3	2.538	2074-53437-0207	1383.77 ± 85.90	-1.31 ± 0.02	6.93 ± 0.66
045	02	J074221.38+165740.3	2.538	2915-54497-0216	1553.70 ± 96.80	-1.25 ± 0.02	5.10 ± 0.68
046	01	J074818.62+272304.7	2.344	2075-53737-0043	658.23 ± 76.70	-1.29 ± 0.04	7.46 ± 1.24
046	02	J074818.62+272304.7	2.344	2075-53730-0055	679.43 ± 58.28	-1.31 ± 0.03	7.36 ± 0.94
047	01	J075007.63+275708.0	2.364	1059-52618-0071	2710.02 ± 128.52	-1.36 ± 0.02	23.93 ± 0.62
047	02	J075007.63+275708.0	2.364	2075-53737-0550	1799.98 ± 68.30	-1.03 ± 0.02	29.12 ± 0.50
048	01	J080049.70+092830.7	2.182	2419-54139-0262	1248.89 ± 130.64	-1.26 ± 0.04	9.03 ± 1.15
048	02	J080049.70+092830.7	2.182	2945-54505-0638	1316.89 ± 72.55	-1.17 ± 0.02	11.08 ± 0.60
049	01	J080455.90+231501.8	2.162	1265-52705-0187	1467.36 ± 153.08	-1.13 ± 0.04	16.28 ± 1.08
049	02	J080455.90+231501.8	2.162	1584-52943-0337	1544.43 ± 107.60	-1.53 ± 0.03	15.41 ± 0.75
050	01	J081213.95+431715.9	1.742	0546-52205-0403	2010.89 ± 109.20	-1.68 ± 0.06	73.49 ± 0.70
050	02	J081213.95+431715.9	1.742	0547-51959-0284	2059.06 ± 94.30	-1.68 ± 0.06	75.13 ± 0.61
051	01	J081822.63+434633.8	2.042	0547-51959-0122	2322.17 ± 177.45	-1.28 ± 0.03	2.78 ± 0.87
051	02	J081822.63+434633.8	2.042	0547-52207-0157	1937.76 ± 107.42	-1.26 ± 0.02	8.13 ± 0.61
052	01	J082238.64+420925.7	1.968	0761-52266-0244	670.99 ± 81.22	-0.69 ± 0.06	7.56 ± 1.44
052	02	J082238.64+420925.7	1.968	0761-54524-0279	1100.38 ± 147.55	-1.81 ± 0.09	3.73 ± 0.99
053	01	J083925.61+045420.2	2.447	1187-52708-0137	949.11 ± 126.67	1.14 ± 0.10	42.31 ± 1.67
053	02	J083925.61+045420.2	2.447	1188-52650-0390	1058.86 ± 121.28	1.48 ± 0.10	41.67 ± 1.38
054	01	J084255.92+223431.9	2.714	2084-53360-0502	2138.52 ± 229.21	-1.02 ± 0.03	19.41 ± 1.17
054	02	J084255.92+223431.9	2.714	3373-54940-0062	2407.33 ± 134.97	-1.25 ± 0.02	12.08 ± 0.59
055	01	J090241.07+571829.0	2.070	0483-51942-0521	708.01 ± 123.95	0.00 ± 0.06	15.65 ± 1.76
055	02	J090241.07+571829.0	2.070	0483-51902-0554	692.91 ± 82.68	-0.05 ± 0.05	18.90 ± 1.26
056	01	J091512.53+305014.9	1.983	1938-53379-0383	1209.80 ± 108.77	-1.12 ± 0.04	4.57 ± 0.96
056	02	J091512.53+305014.9	1.983	2401-53768-0472	1287.03 ± 62.89	-1.13 ± 0.02	4.05 ± 0.52
057	01	J092015.68+350040.5	1.916	1273-52993-0630	1187.70 ± 107.89	-1.28 ± 0.06	27.79 ± 0.95
057	02	J092015.68+350040.5	1.916	1274-52995-0284	1090.35 ± 99.96	-1.34 ± 0.06	28.18 ± 0.96
058	01	J092527.71+151416.9	1.968	2440-53818-0622	1039.65 ± 96.15	-1.39 ± 0.05	14.58 ± 1.06
058	02	J092527.71+151416.9	1.968	3192-54829-0504	1268.01 ± 61.49	-1.47 ± 0.02	8.45 ± 0.57
059	01	J092720.29+101627.0	1.929	1740-53050-0065	983.36 ± 103.77	-2.25 ± 0.08	35.81 ± 1.37
059	02	J092720.29+101627.0	1.929	3319-54915-0425	796.30 ± 43.66	-1.10 ± 0.04	34.60 ± 0.74
060	01	J093300.21+544905.2	1.825	0556-51991-0313	925.17 ± 103.13	-1.09 ± 0.09	10.55 ± 1.34
060	02	J093300.21+544905.2	1.825	0555-52266-0154	919.61 ± 84.46	-1.62 ± 0.08	7.42 ± 1.05
061	01	J093333.29+410522.8	2.153	0940-52670-0287	2118.21 ± 226.18	-1.12 ± 0.04	7.87 ± 1.08
061	02	J093333.29+410522.8	2.153	0939-52636-0034	2275.52 ± 138.07	-1.06 ± 0.02	6.47 ± 0.65

Table 2. – continue

No. (1)	epoch (2)	name (3)	z (4)	Plate-MJD-Fiber (5)	L_{1500} (6)	α (7)	BAL EW (8)
062	01	J093548.50+363121.9	2.977	1275-52996-0145	2526.87 ± 224.46	-1.42 ± 0.03	20.97 ± 1.04
062	02	J093548.50+363121.9	2.977	3223-54865-0303	2310.33 ± 159.98	-1.04 ± 0.02	33.81 ± 0.76
063	01	J093620.52+004649.2	1.719	0476-52027-0442	1099.22 ± 173.80	-1.34 ± 0.10	4.75 ± 1.67
063	02	J093620.52+004649.2	1.719	0476-52314-0444	772.49 ± 110.71	-0.91 ± 0.09	6.41 ± 1.51
064	01	J093859.27+150118.6	2.193	2581-54085-0228	1379.40 ± 142.56	-0.83 ± 0.04	4.16 ± 1.12
064	02	J093859.27+150118.6	2.193	3196-54834-0640	1802.93 ± 83.73	-0.74 ± 0.02	1.28 ± 0.48
065	01	J094338.21-010019.3	2.377	0266-51630-0124	1639.51 ± 149.56	-0.77 ± 0.04	30.02 ± 0.97
065	02	J094338.21-010019.3	2.377	0266-51602-0131	1723.56 ± 150.00	-0.92 ± 0.03	31.13 ± 0.93
066	01	J094425.46+610934.4	2.271	0486-51910-0120	1121.96 ± 112.69	-0.55 ± 0.04	35.61 ± 1.08
066	02	J094425.46+610934.4	2.271	2403-53795-0124	1171.95 ± 60.84	-1.23 ± 0.02	32.36 ± 0.52
067	01	J094456.75+544117.9	1.895	0769-54530-0327	785.66 ± 85.51	-0.60 ± 0.07	6.59 ± 1.14
067	02	J094456.75+544117.9	1.895	3169-54821-0377	698.54 ± 78.91	-0.29 ± 0.06	5.57 ± 1.15
068	01	J094602.23+380059.3	2.068	1276-53035-0160	1675.13 ± 130.50	-1.23 ± 0.03	21.74 ± 0.83
068	02	J094602.23+380059.3	2.068	3223-54865-0566	1599.50 ± 76.83	-0.85 ± 0.02	23.75 ± 0.52
069	01	J095357.00+040039.2	2.427	0571-52286-0560	1310.91 ± 134.76	-0.93 ± 0.03	19.92 ± 1.12
069	02	J095357.00+040039.2	2.427	0572-52289-0312	1306.36 ± 127.44	-1.09 ± 0.03	20.38 ± 1.06
070	01	J095901.24+550408.2	2.180	0945-52652-0436	1194.36 ± 79.91	-0.89 ± 0.03	19.17 ± 0.87
070	02	J095901.24+550408.2	2.180	3169-54821-0627	1675.41 ± 71.33	-1.39 ± 0.02	12.73 ± 0.55
071	01	J100109.51+133433.6	1.841	2584-54153-0020	1428.41 ± 119.67	-0.71 ± 0.06	4.96 ± 0.91
071	02	J100109.51+133433.6	1.841	3248-54880-0120	1554.03 ± 87.20	-0.97 ± 0.04	5.13 ± 0.58
072	01	J100318.99+521506.3	3.325	0903-52385-0177	3897.33 ± 280.68	-1.70 ± 0.04	23.17 ± 0.87
072	02	J100318.99+521506.3	3.325	0903-52400-0179	3813.42 ± 235.67	-1.62 ± 0.03	22.77 ± 0.94
073	01	J100619.31+625334.9	2.001	0487-51943-0077	899.42 ± 91.37	-1.05 ± 0.04	36.20 ± 1.08
073	02	J100619.31+625334.9	2.001	3294-54918-0102	715.36 ± 67.37	-1.53 ± 0.05	30.09 ± 1.06
074	01	J100716.69+030438.6	2.124	0501-52235-0606	2689.48 ± 125.81	-1.23 ± 0.02	6.36 ± 0.48
074	02	J100716.69+030438.6	2.124	3257-54888-0474	1927.77 ± 83.14	-0.91 ± 0.02	10.64 ± 0.44
075	01	J100912.49+252055.2	2.205	2406-54084-0170	793.51 ± 60.54	-0.85 ± 0.03	34.54 ± 0.85
075	02	J100912.49+252055.2	2.205	2347-53757-0213	861.28 ± 119.16	-0.71 ± 0.05	31.59 ± 1.54
076	01	J101425.11+032003.7	2.145	0574-52347-0212	3739.76 ± 177.15	-1.42 ± 0.02	7.23 ± 0.51
076	02	J101425.11+032003.7	2.145	0574-52366-0218	4422.25 ± 214.56	-1.42 ± 0.02	7.33 ± 0.48
077	01	J101542.04+430455.6	2.420	1218-52709-0514	5537.78 ± 244.90	-1.55 ± 0.01	8.24 ± 0.46
077	02	J101542.04+430455.6	2.420	3287-54941-0433	4284.78 ± 154.82	-1.02 ± 0.01	12.99 ± 0.36
078	01	J101616.34+383817.3	1.953	1427-52996-0479	853.61 ± 65.06	-0.89 ± 0.04	49.94 ± 0.88
078	02	J101616.34+383817.3	1.953	3262-54884-0356	1008.76 ± 62.58	-0.59 ± 0.04	54.69 ± 0.70
079	01	J102106.78+303137.5	3.061	2351-53772-0409	2114.50 ± 168.99	-1.97 ± 0.03	7.78 ± 1.01
079	02	J102106.78+303137.5	3.061	2351-53786-0409	2376.23 ± 254.61	-2.01 ± 0.04	10.03 ± 1.23
080	01	J102156.84+282735.8	1.880	2351-53772-0128	610.67 ± 77.81	-0.80 ± 0.09	26.23 ± 1.33
080	02	J102156.84+282735.8	1.880	3260-54883-0624	542.65 ± 55.27	-0.93 ± 0.08	28.45 ± 1.04
081	01	J102250.16+483631.1	2.069	0873-52347-0522	1121.23 ± 91.69	-1.01 ± 0.04	31.33 ± 1.03
081	02	J102250.16+483631.1	2.069	0873-52674-0555	1373.20 ± 95.84	-1.43 ± 0.03	30.29 ± 0.87
082	01	J102754.03+182221.6	3.078	2591-54140-0453	2578.13 ± 231.53	-1.20 ± 0.03	27.76 ± 1.00
082	02	J102754.03+182221.6	3.078	2868-54451-0518	2370.06 ± 84.24	-1.07 ± 0.02	31.29 ± 0.46
083	01	J103006.62+271325.9	1.734	2353-53794-0164	871.74 ± 99.58	-0.60 ± 0.08	41.39 ± 1.29
083	02	J103006.62+271325.9	1.734	3261-54881-0582	893.54 ± 43.96	-0.94 ± 0.05	43.90 ± 0.60
084	01	J104010.46+432811.6	2.595	2567-54179-0020	2204.80 ± 105.51	-1.21 ± 0.02	20.61 ± 0.59
084	02	J104010.46+432811.6	2.595	3258-54884-0219	1708.79 ± 115.30	-0.98 ± 0.02	20.60 ± 0.83
085	01	J104945.36+285823.3	2.154	2359-53800-0332	732.44 ± 101.18	-0.15 ± 0.05	42.83 ± 1.42
085	02	J104945.36+285823.3	2.154	2359-53826-0332	764.55 ± 112.34	-0.18 ± 0.05	42.27 ± 1.48
086	01	J105012.58+001158.8	2.206	2409-54210-0538	366.41 ± 38.80	-0.38 ± 0.04	5.27 ± 1.19
086	02	J105012.58+001158.8	2.206	2569-54234-0554	445.01 ± 48.59	-0.71 ± 0.04	6.90 ± 1.21
087	01	J105416.51+512326.0	2.340	0876-52669-0533	1799.34 ± 142.16	-1.56 ± 0.03	10.81 ± 0.86
087	02	J105416.51+512326.0	2.340	0876-52346-0535	1548.09 ± 107.72	-1.30 ± 0.02	9.26 ± 0.78
088	01	J105657.54+492957.9	2.162	0876-52669-0014	2073.65 ± 172.16	-1.03 ± 0.03	1.91 ± 0.88
088	02	J105657.54+492957.9	2.162	0876-52346-0017	1211.93 ± 138.04	-1.67 ± 0.04	0.97 ± 1.20
089	01	J110015.55+271451.7	3.339	2359-53800-0003	3164.53 ± 191.43	-1.22 ± 0.04	22.14 ± 0.79
089	02	J110015.55+271451.7	3.339	2359-53826-0003	3247.59 ± 170.00	-1.19 ± 0.04	21.17 ± 0.82
090	01	J110152.91+275838.6	2.865	2211-53786-0256	2034.26 ± 323.16	-0.26 ± 0.04	8.94 ± 1.42
090	02	J110152.91+275838.6	2.865	2870-54534-0165	2008.90 ± 132.62	-0.11 ± 0.02	6.97 ± 0.72
091	01	J110208.59+660156.5	2.064	0490-51929-0142	897.03 ± 75.33	-1.14 ± 0.04	24.04 ± 0.89
091	02	J110208.59+660156.5	2.064	3171-54862-0164	1034.75 ± 68.61	-1.04 ± 0.03	18.57 ± 0.69
092	01	J110427.08+054848.3	3.006	0581-52353-0328	2714.96 ± 233.04	-2.29 ± 0.03	4.70 ± 1.12
092	02	J110427.08+054848.3	3.006	0581-52356-0328	2849.43 ± 230.02	-2.23 ± 0.03	4.87 ± 1.03

Table 2. – continue

No. (1)	epoch (2)	name (3)	z (4)	Plate-MJD-Fiber (5)	L_{1500} (6)	α (7)	BAL EW (8)
093	01	J111313.29+102212.4	2.247	1222-52763-0322	4914.87 ± 252.26	-0.99 ± 0.02	8.25 ± 0.53
093	02	J111313.29+102212.4	2.247	2393-54156-0420	6065.31 ± 123.81	-1.08 ± 0.01	7.90 ± 0.22
094	01	J111651.98+463508.6	1.888	3216-54908-0385	540.64 ± 62.58	-1.52 ± 0.08	14.73 ± 1.18
094	02	J111651.98+463508.6	1.888	3216-54853-0399	581.58 ± 51.68	-1.41 ± 0.06	11.95 ± 0.98
095	01	J112239.20+602012.3	2.227	0951-52398-0523	1142.37 ± 128.40	-1.50 ± 0.04	9.10 ± 1.17
095	02	J112239.20+602012.3	2.227	3328-54964-0081	966.08 ± 94.23	-1.73 ± 0.03	5.71 ± 0.93
096	01	J112258.77+164540.3	3.031	2499-54176-0308	8025.55 ± 284.56	-1.04 ± 0.03	42.12 ± 0.45
096	02	J112258.77+164540.3	3.031	3327-54951-0153	7874.83 ± 162.16	-0.81 ± 0.03	39.93 ± 0.30
097	01	J112703.06+450516.4	1.857	1366-53063-0321	1130.13 ± 113.64	-1.85 ± 0.10	20.09 ± 1.06
097	02	J112703.06+450516.4	1.857	3215-54861-0399	671.43 ± 50.17	-1.64 ± 0.07	12.46 ± 0.78
098	01	J112939.84+600728.9	1.724	0952-52409-0412	1091.60 ± 108.85	-1.44 ± 0.07	5.73 ± 1.11
098	02	J112939.84+600728.9	1.724	3211-54852-0424	1024.48 ± 71.53	-1.71 ± 0.05	2.00 ± 0.77
099	01	J113529.56+584803.8	1.781	0952-52409-0150	778.03 ± 98.26	-1.23 ± 0.09	21.69 ± 1.36
099	02	J113529.56+584803.8	1.781	2881-54502-0296	672.88 ± 82.21	-1.60 ± 0.09	30.81 ± 1.37
100	01	J113621.05+005021.2	3.428	0282-51630-0535	8531.06 ± 370.79	-1.77 ± 0.02	6.83 ± 0.46
100	02	J113621.05+005021.2	3.428	0282-51658-0535	8891.49 ± 282.79	-1.71 ± 0.02	6.31 ± 0.38
101	01	J115944.82+011206.9	2.002	0285-51663-0530	5261.82 ± 266.65	-2.11 ± 0.02	18.10 ± 0.53
101	02	J115944.82+011206.9	2.002	0285-51930-0540	4932.98 ± 191.60	-1.67 ± 0.02	18.12 ± 0.40
102	01	J120217.29+332108.7	2.252	2089-53498-0292	1772.50 ± 118.41	-1.64 ± 0.02	8.47 ± 0.71
102	02	J120217.29+332108.7	2.252	2095-53474-0448	1800.74 ± 181.35	-1.57 ± 0.03	9.41 ± 0.97
103	01	J120653.39+492919.3	1.845	0969-52442-0107	2508.88 ± 130.53	-1.71 ± 0.05	64.15 ± 0.55
103	02	J120653.39+492919.3	1.845	2919-54537-0170	2198.63 ± 58.20	-1.55 ± 0.03	59.46 ± 0.28
104	01	J120822.25+302423.9	2.252	2230-53799-0353	2827.30 ± 216.24	-1.43 ± 0.02	5.31 ± 0.73
104	02	J120822.25+302423.9	2.252	3181-54860-0025	2552.20 ± 118.31	-1.21 ± 0.01	1.68 ± 0.49
105	01	J121147.38+203402.4	2.413	2610-54476-0341	2679.76 ± 197.05	-1.69 ± 0.03	23.20 ± 0.82
105	02	J121147.38+203402.4	2.413	2918-54554-0622	2761.27 ± 93.74	-1.76 ± 0.01	17.27 ± 0.39
106	01	J121328.78-025617.8	2.153	0332-52367-0065	2299.24 ± 184.48	-1.11 ± 0.03	13.76 ± 0.85
106	02	J121328.78-025617.8	2.153	0333-52313-0315	2302.60 ± 149.92	-1.19 ± 0.03	11.93 ± 0.73
107	01	J122604.28+034317.8	1.767	0519-52283-0565	1956.38 ± 109.69	-1.37 ± 0.05	20.78 ± 0.58
107	02	J122604.28+034317.8	1.767	3253-54941-0202	2113.96 ± 101.23	-1.31 ± 0.03	21.63 ± 0.50
108	01	J122951.77+351929.9	1.821	2010-53495-0309	1731.18 ± 116.99	-1.42 ± 0.06	18.34 ± 0.79
108	02	J122951.77+351929.9	1.821	3395-55004-0278	1623.91 ± 80.70	-1.66 ± 0.04	14.79 ± 0.55
109	01	J123303.50+620915.9	1.839	0780-52370-0109	1419.77 ± 122.12	-1.45 ± 0.07	18.91 ± 0.89
109	02	J123303.50+620915.9	1.839	0781-52373-0278	1502.92 ± 152.26	-1.52 ± 0.08	19.42 ± 1.08
110	01	J123411.74+615832.5	1.949	0780-52370-0065	1047.71 ± 127.36	-1.04 ± 0.07	40.59 ± 1.32
110	02	J123411.74+615832.5	1.949	0781-52373-0275	958.88 ± 113.42	-0.73 ± 0.07	38.02 ± 1.29
111	01	J123736.42+143640.1	2.704	1768-53442-0038	2075.61 ± 219.11	-1.00 ± 0.03	31.35 ± 1.25
111	02	J123736.42+143640.1	2.704	3254-54889-0548	2426.53 ± 129.76	-1.23 ± 0.02	31.44 ± 0.63
112	01	J124140.08+131746.1	2.143	1694-53472-0336	1303.73 ± 120.77	-1.37 ± 0.04	10.71 ± 1.07
112	02	J124140.08+131746.1	2.143	3255-54885-0205	1096.03 ± 72.40	-1.21 ± 0.02	13.47 ± 0.65
113	01	J124551.44+010505.0	2.809	0291-51660-0607	4162.68 ± 267.66	-1.54 ± 0.02	29.94 ± 0.92
113	02	J124551.44+010505.0	2.809	0291-51928-0612	3921.53 ± 236.91	-1.61 ± 0.02	29.11 ± 0.78
114	01	J125950.76+183236.1	2.248	2616-54499-0124	1083.87 ± 122.29	-1.04 ± 0.04	3.88 ± 1.22
114	02	J125950.76+183236.1	2.248	2924-54582-0083	1031.82 ± 71.36	-0.92 ± 0.02	2.58 ± 0.76
115	01	J130136.12+000157.9	1.783	0293-51994-0074	3457.46 ± 161.29	-1.54 ± 0.05	35.63 ± 0.56
115	02	J130136.12+000157.9	1.783	0293-51689-0079	3261.62 ± 129.30	-1.72 ± 0.04	35.73 ± 0.47
116	01	J130221.80-004638.2	2.704	0293-51689-0012	2020.28 ± 259.70	-0.83 ± 0.04	19.90 ± 1.76
116	02	J130221.80-004638.2	2.704	0293-51994-0015	1901.44 ± 217.58	-0.92 ± 0.04	14.52 ± 1.74
117	01	J131416.43-015020.9	2.180	0340-51691-0508	1280.93 ± 155.59	-1.65 ± 0.04	7.17 ± 1.30
117	02	J131416.43-015020.9	2.180	0340-51990-0514	1386.06 ± 116.92	-1.86 ± 0.03	5.04 ± 0.93
118	01	J131433.83+032321.9	2.255	0525-52029-0572	2105.90 ± 201.20	-1.75 ± 0.03	5.48 ± 1.01
118	02	J131433.83+032321.9	2.255	0525-52295-0576	1720.59 ± 137.72	-1.46 ± 0.02	11.15 ± 0.81
119	01	J131505.89+590157.5	1.932	0958-52410-0157	2256.73 ± 137.19	-0.90 ± 0.04	25.40 ± 0.71
119	02	J131505.89+590157.5	1.932	3237-54883-0067	1889.68 ± 78.10	-0.63 ± 0.02	20.72 ± 0.46
120	01	J131714.21+010013.0	2.698	0296-51578-0327	3857.85 ± 267.72	-1.61 ± 0.03	23.92 ± 0.88
120	02	J131714.21+010013.0	2.698	0296-51984-0329	3796.38 ± 215.64	-1.55 ± 0.02	26.54 ± 0.76
121	01	J131853.45+002211.5	2.074	0296-51578-0383	1530.04 ± 143.96	-1.60 ± 0.04	19.34 ± 1.00
121	02	J131853.45+002211.5	2.074	0296-51984-0390	1372.49 ± 130.93	-1.47 ± 0.03	21.71 ± 0.99
122	01	J131905.95+660415.7	1.710	0496-51973-0260	1544.80 ± 169.04	-2.24 ± 0.08	9.63 ± 1.14
122	02	J131905.95+660415.7	1.710	0496-51988-0260	1415.09 ± 161.92	-1.78 ± 0.07	7.41 ± 1.15
123	01	J132304.58-003856.5	1.827	0296-51578-0074	1363.05 ± 108.92	-1.36 ± 0.07	25.33 ± 1.04
123	02	J132304.58-003856.5	1.827	0296-51984-0076	1328.15 ± 113.27	-1.11 ± 0.07	22.89 ± 1.08

Table 2. – continue

No. (1)	epoch (2)	name (3)	z (4)	Plate-MJD-Fiber (5)	L_{1500} (6)	α (7)	BAL EW (8)
124	01	J132422.54+245222.4	2.363	2664-54524-0537	3194.67 ± 168.12	-1.38 ± 0.02	28.43 ± 0.56
124	02	J132422.54+245222.4	2.363	3303-54950-0599	2773.42 ± 102.74	-1.36 ± 0.01	27.57 ± 0.37
125	01	J132827.06+581836.8	3.139	0960-52466-0304	2794.53 ± 251.42	-1.76 ± 0.05	11.45 ± 1.38
125	02	J132827.06+581836.8	3.139	0960-52425-0318	2827.13 ± 188.18	-2.15 ± 0.04	14.99 ± 0.87
126	01	J133138.50+004221.1	2.424	0298-51955-0374	2264.05 ± 164.18	-1.82 ± 0.02	11.14 ± 0.78
126	02	J133138.50+004221.1	2.424	0298-51662-0376	2168.88 ± 208.04	-1.62 ± 0.03	6.24 ± 1.10
127	01	J133514.39+531805.8	1.874	1041-52724-0039	1578.48 ± 127.97	-1.17 ± 0.06	13.08 ± 0.91
127	02	J133514.39+531805.8	1.874	3318-54951-0115	1395.43 ± 83.67	-0.99 ± 0.04	14.02 ± 0.63
128	01	J134101.28+083755.7	2.494	1804-53886-0318	1512.42 ± 144.88	0.30 ± 0.08	53.75 ± 1.08
128	02	J134101.28+083755.7	2.494	2928-54614-0128	1427.07 ± 68.11	-0.06 ± 0.05	56.01 ± 0.52
129	01	J134544.55+002810.7	2.453	0300-51943-0382	1918.11 ± 151.67	-1.34 ± 0.03	20.84 ± 0.90
129	02	J134544.55+002810.7	2.453	0300-51666-0426	2153.34 ± 160.97	-1.65 ± 0.03	17.78 ± 0.83
130	01	J135448.04+501137.9	2.141	1670-54553-0483	722.58 ± 85.80	-0.57 ± 0.05	11.40 ± 1.31
130	02	J135448.04+501137.9	2.141	1670-53438-0486	771.58 ± 81.16	-0.76 ± 0.04	5.88 ± 1.16
131	01	J135559.03-002413.6	2.337	0301-51641-0266	3095.13 ± 179.97	-1.68 ± 0.02	14.60 ± 0.65
131	02	J135559.03-002413.6	2.337	0301-51942-0267	2769.95 ± 162.58	-1.72 ± 0.02	15.86 ± 0.67
132	01	J135721.77+005501.1	1.997	0301-51942-0408	2278.58 ± 128.98	-1.27 ± 0.02	8.54 ± 0.59
132	02	J135721.77+005501.1	1.997	0301-51641-0411	2084.64 ± 133.82	-1.31 ± 0.03	8.32 ± 0.66
133	01	J135941.58+000851.9	1.736	0301-51942-0517	862.52 ± 97.91	-1.72 ± 0.08	5.32 ± 1.17
133	02	J135941.58+000851.9	1.736	0301-51641-0520	857.03 ± 94.83	-1.39 ± 0.09	7.58 ± 1.28
134	01	J142333.56+573909.5	1.870	0789-52342-0229	789.71 ± 102.50	-0.73 ± 0.10	25.77 ± 1.49
134	02	J142333.56+573909.5	1.870	2547-53917-0265	735.62 ± 110.03	-0.08 ± 0.11	24.84 ± 1.74
135	01	J142910.55+634603.6	1.886	0499-51988-0143	686.52 ± 76.90	-1.47 ± 0.08	9.11 ± 1.24
135	02	J142910.55+634603.6	1.886	2947-54533-0327	522.58 ± 63.00	-1.34 ± 0.09	10.04 ± 1.34
136	01	J143117.07+632701.7	1.891	0499-51988-0105	1828.02 ± 94.61	-1.04 ± 0.03	15.91 ± 0.54
136	02	J143117.07+632701.7	1.891	2947-54533-0370	1876.33 ± 135.72	-1.41 ± 0.05	11.06 ± 0.75
137	01	J143130.03+570138.8	1.797	0790-52441-0245	2142.59 ± 140.70	-1.74 ± 0.06	23.75 ± 0.80
137	02	J143130.03+570138.8	1.797	0790-52346-0257	2224.85 ± 146.92	-1.96 ± 0.06	25.38 ± 0.75
138	01	J143307.40+003319.0	2.744	0306-51637-0546	1573.84 ± 179.18	-1.87 ± 0.04	17.83 ± 1.57
138	02	J143307.40+003319.0	2.744	0306-51690-0558	1552.12 ± 176.33	-1.77 ± 0.04	17.49 ± 1.84
139	01	J143612.69+443812.6	1.848	1288-52731-0105	896.37 ± 125.93	-0.62 ± 0.10	18.20 ± 1.50
139	02	J143612.69+443812.6	1.848	1289-52734-0350	930.19 ± 111.76	-0.51 ± 0.09	14.97 ± 1.30
140	01	J143641.24+001558.9	1.867	0306-51637-0628	1072.35 ± 87.18	-1.19 ± 0.08	28.91 ± 0.97
140	02	J143641.24+001558.9	1.867	0306-51690-0629	1058.77 ± 106.35	-1.32 ± 0.09	31.47 ± 1.17
141	01	J143758.06+011119.5	2.045	0307-51663-0443	1022.18 ± 114.78	-0.66 ± 0.04	24.68 ± 1.18
141	02	J143758.06+011119.5	2.045	0536-52024-0217	1014.26 ± 113.98	-0.80 ± 0.04	26.18 ± 1.20
142	01	J143907.51-010616.7	1.819	0307-51663-0089	539.73 ± 116.89	-0.27 ± 0.14	12.58 ± 2.53
142	02	J143907.51-010616.7	1.819	0919-52409-0566	674.14 ± 115.50	-0.35 ± 0.11	10.88 ± 1.90
143	01	J144136.54+632519.4	1.779	0609-52339-0322	1067.87 ± 136.16	-1.70 ± 0.10	13.63 ± 1.38
143	02	J144136.54+632519.4	1.779	2947-54533-0153	730.82 ± 76.55	-2.36 ± 0.08	7.84 ± 1.23
144	01	J144351.38+560325.6	2.275	0791-52347-0247	1532.55 ± 145.80	-1.60 ± 0.03	11.38 ± 1.07
144	02	J144351.38+560325.6	2.275	0791-52435-0247	1632.08 ± 169.46	-1.62 ± 0.04	10.54 ± 1.15
145	01	J144412.36+582636.9	2.336	0790-52441-0583	1187.20 ± 149.14	-0.58 ± 0.04	2.63 ± 1.32
145	02	J144412.36+582636.9	2.336	0790-52346-0584	1329.29 ± 158.70	-0.95 ± 0.04	5.10 ± 1.31
146	01	J144514.86-002358.1	2.237	2934-54626-0223	3403.12 ± 95.96	0.21 ± 0.02	24.90 ± 0.27
146	02	J144514.86-002358.1	2.237	2909-54653-0222	3109.81 ± 142.56	0.21 ± 0.02	24.98 ± 0.48
147	01	J144935.96+631836.0	1.735	0609-52339-0538	891.96 ± 130.81	-1.12 ± 0.10	17.81 ± 1.66
147	02	J144935.96+631836.0	1.735	2947-54533-0044	615.93 ± 76.12	-1.45 ± 0.08	16.42 ± 1.51
148	01	J145110.68+040925.2	1.732	0588-52029-0440	1295.74 ± 167.75	-1.52 ± 0.09	19.43 ± 1.37
148	02	J145110.68+040925.2	1.732	0588-52045-0440	1408.12 ± 120.28	-1.66 ± 0.07	19.36 ± 0.93
149	01	J145353.45+040124.0	2.088	0588-52029-0488	1917.34 ± 147.12	-1.69 ± 0.03	10.69 ± 0.99
149	02	J145353.45+040124.0	2.088	0588-52045-0496	2106.68 ± 102.42	-1.82 ± 0.02	10.19 ± 0.70
150	01	J145943.02+010601.5	2.092	0310-51616-0393	2071.46 ± 188.94	-0.97 ± 0.03	2.97 ± 0.97
150	02	J145943.02+010601.5	2.092	0538-52029-0012	2210.66 ± 160.70	-1.58 ± 0.03	3.39 ± 0.79
151	01	J150033.52+003353.6	2.438	0310-51616-0363	3455.47 ± 259.64	-1.11 ± 0.02	12.07 ± 0.78
151	02	J150033.52+003353.6	2.438	0310-51990-0388	2449.34 ± 197.15	-0.53 ± 0.03	18.26 ± 0.83
152	01	J150332.93+440120.6	2.049	1676-53147-0028	1118.21 ± 104.63	-0.68 ± 0.04	16.02 ± 1.19
152	02	J150332.93+440120.6	2.049	1677-53148-0358	1205.95 ± 91.43	-0.83 ± 0.04	18.93 ± 1.02
153	01	J150428.59-002015.9	1.865	0310-51616-0170	1359.99 ± 154.39	-1.30 ± 0.09	9.28 ± 1.28
153	02	J150428.59-002015.9	1.865	0310-51990-0199	1261.01 ± 131.14	-1.34 ± 0.08	9.30 ± 1.12
154	01	J150659.88+420652.7	1.868	1291-52735-0489	1156.12 ± 101.45	-1.54 ± 0.08	14.99 ± 1.00
154	02	J150659.88+420652.7	1.868	1291-52738-0489	1187.00 ± 112.53	-1.65 ± 0.08	16.55 ± 1.03

Table 2. – continue

No. (1)	epoch (2)	name (3)	z (4)	Plate-MJD-Fiber (5)	L_{1500} (6)	α (7)	BAL EW (8)
155	01	J152057.81+461641.3	1.962	1050-52721-0629	648.26 ± 113.38	0.72 ± 0.07	55.97 ± 1.92
155	02	J152057.81+461641.3	1.962	1331-52766-0248	630.92 ± 91.87	0.39 ± 0.08	60.70 ± 1.73
156	01	J152149.78+010236.4	2.231	0313-51673-0339	1365.55 ± 164.68	-1.48 ± 0.04	6.09 ± 1.25
156	02	J152149.78+010236.4	2.231	2953-54560-0209	2686.50 ± 183.33	-1.83 ± 0.02	3.84 ± 0.70
157	01	J153045.76+383952.3	2.022	1293-52765-0068	2835.80 ± 153.79	-1.74 ± 0.02	16.74 ± 0.54
157	02	J153045.76+383952.3	2.022	1294-52753-0329	2418.72 ± 167.68	-1.36 ± 0.03	14.27 ± 0.75
158	01	J153715.74+582933.9	2.590	0615-52345-0577	6004.06 ± 393.01	-0.68 ± 0.02	16.86 ± 0.59
158	02	J153715.74+582933.9	2.590	0615-52347-0585	6259.21 ± 269.68	-0.75 ± 0.01	16.87 ± 0.42
159	01	J154359.43+535903.1	2.371	0616-52374-0097	6736.25 ± 391.38	-1.73 ± 0.02	4.99 ± 0.68
159	02	J154359.43+535903.1	2.371	0616-52442-0120	6930.08 ± 274.79	-1.56 ± 0.01	4.20 ± 0.41
160	01	J160649.23+451051.6	2.826	0814-52370-0355	2815.78 ± 261.00	-0.58 ± 0.03	17.28 ± 1.31
160	02	J160649.23+451051.6	2.826	0814-52443-0359	2792.49 ± 275.76	-0.60 ± 0.03	18.92 ± 1.31
161	01	J163023.69+390841.7	2.008	1172-52759-0008	881.66 ± 139.10	-0.03 ± 0.06	14.28 ± 1.58
161	02	J163023.69+390841.7	2.008	1173-52790-0453	790.73 ± 134.68	0.09 ± 0.07	12.60 ± 1.91
162	01	J164419.97+274447.0	3.068	1690-53475-0350	5126.54 ± 224.13	-1.39 ± 0.02	24.99 ± 0.59
162	02	J164419.97+274447.0	3.068	2949-54557-0603	4163.99 ± 231.63	-1.70 ± 0.02	27.11 ± 0.65
163	01	J164424.98+274136.5	3.893	1690-53475-0342	9125.81 ± 840.91	-1.07 ± 0.03	5.79 ± 0.57
163	02	J164424.98+274136.5	3.893	2949-54557-0602	7408.34 ± 746.56	-1.33 ± 0.03	4.58 ± 0.60
164	01	J165443.30+372008.0	1.928	0632-52071-0125	1332.06 ± 136.03	-1.58 ± 0.05	3.47 ± 1.06
164	02	J165443.30+372008.0	1.928	0820-52438-0371	1157.64 ± 93.21	-1.79 ± 0.05	3.72 ± 0.89
165	01	J165631.20+353259.0	2.039	0819-52409-0006	857.54 ± 126.85	-0.30 ± 0.06	32.15 ± 1.58
165	02	J165631.20+353259.0	2.039	0820-52438-0092	1036.77 ± 87.36	-0.80 ± 0.04	35.35 ± 0.94
166	01	J170105.08+372347.3	1.959	0820-52438-0614	796.09 ± 108.81	-0.73 ± 0.06	18.23 ± 1.29
166	02	J170105.08+372347.3	1.959	0820-52405-0638	838.88 ± 97.70	-1.10 ± 0.06	16.51 ± 1.26
167	01	J170633.06+615715.1	2.012	0351-51780-0555	1272.88 ± 127.51	-1.76 ± 0.04	9.93 ± 1.12
167	02	J170633.06+615715.1	2.012	0351-51695-0556	1321.14 ± 137.66	-1.64 ± 0.04	11.44 ± 0.98
168	01	J170931.00+630357.2	2.395	0352-51789-0310	3799.17 ± 193.13	-1.20 ± 0.02	26.52 ± 0.58
168	02	J170931.00+630357.2	2.395	0352-51694-0311	3023.91 ± 174.46	-0.91 ± 0.03	29.68 ± 0.67
169	01	J171731.04+621912.0	2.118	0352-51789-0209	1199.22 ± 122.94	-1.53 ± 0.04	10.12 ± 1.11
169	02	J171731.04+621912.0	2.118	0352-51694-0215	1113.01 ± 138.59	-1.66 ± 0.05	9.99 ± 1.33
170	01	J172012.40+545601.1	2.100	0357-51813-0189	1923.35 ± 103.37	-1.78 ± 0.02	14.19 ± 0.59
170	02	J172012.40+545601.1	2.100	0367-51997-0184	2071.91 ± 100.37	-2.02 ± 0.02	14.55 ± 0.49
171	01	J173802.90+535047.2	1.918	0362-51999-0134	989.13 ± 113.87	-0.35 ± 0.06	6.12 ± 1.21
171	02	J173802.90+535047.2	1.918	0360-51780-0134	703.79 ± 148.22	0.70 ± 0.10	2.17 ± 2.26
172	01	J212127.78-081737.5	1.906	0640-52178-0286	1276.19 ± 169.68	-0.84 ± 0.06	2.42 ± 1.31
172	02	J212127.78-081737.5	1.906	0640-52200-0295	1189.13 ± 180.42	-0.83 ± 0.08	1.95 ± 1.45
173	01	J213113.93-083913.5	1.983	0641-52176-0297	632.51 ± 115.90	-0.33 ± 0.08	22.50 ± 1.99
173	02	J213113.93-083913.5	1.983	0641-52199-0299	732.44 ± 103.17	-0.65 ± 0.07	22.87 ± 1.63
174	01	J213138.07-002537.8	1.837	0989-52468-0273	591.30 ± 115.95	-0.25 ± 0.13	34.51 ± 2.15
174	02	J213138.07-002537.8	1.837	1963-54331-0238	301.29 ± 44.97	0.36 ± 0.08	17.94 ± 1.60
175	01	J213138.93-070013.4	2.048	0641-52176-0386	1272.71 ± 116.96	-1.55 ± 0.04	29.72 ± 1.07
175	02	J213138.93-070013.4	2.048	0641-52199-0390	1258.61 ± 101.25	-1.46 ± 0.04	32.74 ± 0.97
176	01	J213508.59-075502.1	1.799	0641-52176-0108	1611.66 ± 128.10	-1.45 ± 0.06	6.42 ± 0.94
176	02	J213508.59-075502.1	1.799	0641-52199-0116	1778.34 ± 140.06	-1.71 ± 0.06	8.97 ± 0.93
177	01	J213648.17-001546.6	2.180	0989-52468-0104	1169.71 ± 128.27	-1.46 ± 0.04	13.46 ± 1.23
177	02	J213648.17-001546.6	2.180	1152-52941-0317	1320.84 ± 103.66	-1.42 ± 0.03	8.75 ± 0.83
178	01	J221555.98+010127.0	2.241	1104-52912-0530	1838.20 ± 148.25	-1.66 ± 0.03	13.56 ± 0.87
178	02	J221555.98+010127.0	2.241	3146-54773-0609	1671.33 ± 105.68	-1.21 ± 0.02	8.65 ± 0.66
179	01	J222107.29+125627.2	1.732	0736-52210-0027	1291.86 ± 161.31	-1.06 ± 0.08	24.85 ± 1.38
179	02	J222107.29+125627.2	1.732	0736-52221-0031	1514.98 ± 151.15	-1.48 ± 0.07	23.80 ± 1.06
180	01	J224248.92-085822.8	2.390	0722-52224-0075	1594.81 ± 161.98	-1.80 ± 0.03	11.72 ± 1.03
180	02	J224248.92-085822.8	2.390	0723-52201-0358	1654.45 ± 160.01	-1.78 ± 0.03	11.31 ± 0.96
181	01	J224324.59-005330.7	1.895	0378-52146-0216	1001.88 ± 150.58	-0.65 ± 0.09	19.33 ± 1.58
181	02	J224324.59-005330.7	1.895	0675-52590-0208	1159.24 ± 110.38	-0.78 ± 0.05	17.35 ± 1.03
182	01	J225706.17-002532.8	1.985	0380-51792-0274	519.08 ± 117.48	1.05 ± 0.13	26.30 ± 2.44
182	02	J225706.17-002532.8	1.985	0676-52178-0039	521.97 ± 131.91	1.02 ± 0.12	20.28 ± 2.71
183	01	J231105.54-102837.5	3.194	0726-52226-0130	6948.05 ± 210.14	-1.13 ± 0.02	43.91 ± 0.38
183	02	J231105.54-102837.5	3.194	0726-52207-0133	7419.36 ± 378.42	-1.08 ± 0.03	43.52 ± 0.58
184	01	J231958.70-002449.3	1.890	0382-51816-0064	1329.00 ± 130.74	-0.12 ± 0.06	21.62 ± 1.05
184	02	J231958.70-002449.3	1.890	0680-52200-0261	1562.23 ± 130.52	-0.72 ± 0.06	24.83 ± 0.92
185	01	J232840.99-085315.8	1.729	0646-52523-0446	762.37 ± 100.71	-1.47 ± 0.10	41.52 ± 1.65
185	02	J232840.99-085315.8	1.729	3145-54801-0367	1301.68 ± 46.78	-1.57 ± 0.03	40.79 ± 0.47

Table 2. – continue

No. (1)	epoch (2)	name (3)	z (4)	Plate-MJD-Fiber (5)	L_{1500} (6)	α (7)	BAL EW (8)
186	01	J234711.44-103742.4	1.800	0648-52559-0098	2954.64 ± 116.50	-0.07 ± 0.04	49.98 ± 0.55
186	02	J234711.44-103742.4	1.800	2311-54331-0216	2922.86 ± 71.76	-0.36 ± 0.03	51.92 ± 0.41
187	01	J235702.54-004824.0	3.013	0387-51791-0246	2437.82 ± 209.11	-1.31 ± 0.04	18.02 ± 1.10
187	02	J235702.54-004824.0	3.013	0685-52203-0317	2321.58 ± 213.74	-1.38 ± 0.04	20.08 ± 1.21
188	01	J235859.47-002426.2	1.759	0387-51791-0181	942.02 ± 96.73	-0.98 ± 0.08	15.85 ± 1.25
188	02	J235859.47-002426.2	1.759	0685-52203-0164	760.98 ± 105.55	-0.43 ± 0.09	21.50 ± 1.53

Table 3. The subsample of 43 two-epoch spectra with identified variable BAL regions. Col. (1) is the No. of the two-epoch spectra. Col. (2) is the name. Col. (3) is the redshift. Col. (4) is one observation of Plate-MJD-Fiber. Col. (5) is another observation of Plate-MJD-Fiber. Col. (6) is the bolometric luminosity in units of erg s^{-1} . Col. (7) is the Mg II -based black hole mass in units of $M_{\odot}$. Col. (8) is the Eddington ratio. Col. (9) is ΔEW of all variable BAL regions in two-epoch different spectra in units of Å. Col. (10) is the boundary of all variable BAL regions (V_{max}, V_{min}) in units of km s^{-1} .

N (1)	$name$ (2)	z (3)	Plate-MJD-Fiber[1] (4)	Plate-MJD-Fiber[2] (5)	$LogL_{bol}$ (6)	$LogM_{BH}$ (7)	L_{bol}/L_{Edd} (8)	ΔEW^{vary} (9)	Vary(V_{max}, V_{min}) (10)
001	J002710.06-094435.3	2.070	0653-52145-0556	3105-54825-0310	46.96	8.87 ± 0.19	0.98	-8.45 ± 0.54	(27311.7, 22275.5); (5036.2, 2324.4)
002	J003312.25+155442.4	1.937	0417-51821-0576	3133-54789-0379	46.23	8.86 ± 0.19	0.19	-4.17 ± 0.59	(21113.3, 19951.1); (14333.8, 12203.1)
003	J004527.68+143816.1	1.992	0419-51812-0105	0419-51868-0106	47.44	9.70 ± 0.03	0.43	$+0.61 \pm 0.17$	(7360.6, 6198.4)
004	J005419.99+002727.9	2.490	0394-51876-0514	3111-54800-0509	47.07	–	–	-2.76 ± 0.29	(8329.1, 6585.8); (4455.1, 3099.2)
005	J010859.53-105757.8	1.807	0659-52199-0099	3109-54833-0003	46.74	8.93 ± 0.11	0.51	$+5.03 \pm 0.74$	(28861.3, 27311.7); (21500.7, 20338.5); (11234.6, 10072.4)
006	J012603.62-100114.8	2.302	0661-52163-0114	2878-54465-0274	46.93	–	–	$+2.93 \pm 0.46$	(6585.8, 3292.9)
007	J020006.31-003709.7	2.141	0403-51871-0070	2866-54478-0197	46.65	10.14 ± 0.14	0.03	$+6.68 \pm 0.48$	(20338.5, 18014.1); (16851.9, 13365.3); (12590.5, 11234.6)
008	J021818.14-092153.5	1.880	0668-52162-0218	3122-54821-0201	47.08	9.80 ± 0.13	0.15	$+0.76 \pm 0.21$	(12009.4, 10847.2)
009	J022036.27-081242.9	2.004	0668-52162-0547	3122-54821-0482	46.94	9.24 ± 0.12	0.40	-2.07 ± 0.35	(27311.7, 26149.5); (23825.1, 21888.1)
010	J022349.24+004727.8	2.335	0704-52205-0459	3127-54835-0338	46.43	–	–	$+0.89 \pm 0.35$	(11428.3, 10459.8)
011	J023252.80-001351.1	2.033	0705-52200-0063	3126-54804-0205	46.70	9.24 ± 0.19	0.23	-6.65 ± 0.56	(10266.1, 6585.8); (6198.4, 4261.4)
012	J074221.38+165740.3	2.538	2074-53437-0207	2915-54497-0216	46.94	–	–	-1.20 ± 0.24	(23631.4, 22275.5)
013	J075007.63+275708.0	2.364	1059-52618-0071	2075-53737-0550	46.94	–	–	$+6.43 \pm 0.47$	(23825.1, 18401.5); (10072.4, 6973.2)
014	J080455.90+231501.8	2.162	1265-52705-0187	1584-52943-0337	46.79	9.28 ± 0.23	0.26	-1.92 ± 0.45	(24018.8, 21888.1)
015	J081213.95+431715.9	1.742	0546-52205-0403	0547-51959-0284	46.95	9.37 ± 0.10	0.30	$+4.58 \pm 0.60$	(28086.5, 24212.5)
016	J081822.63+434633.8	2.042	0547-51959-0122	0547-52207-0157	46.97	9.49 ± 0.06	0.24	$+2.95 \pm 0.38$	(13946.4, 10847.2)
017	J082238.64+420925.7	1.968	0761-52266-0244	0761-54524-0279	46.56	9.44 ± 0.12	0.10	-2.78 ± 0.44	(8910.2, 7941.7)
018	J084255.92+223431.9	2.714	2084-53360-0502	3373-54940-0062	46.91	–	–	-4.81 ± 0.60	(20338.5, 16270.8); (15883.4, 14140.1)
019	J092527.71+151416.9	1.968	2440-53818-0622	3192-54829-0504	46.53	9.05 ± 0.21	0.24	-4.62 ± 0.52	(18788.9, 16077.1); (9297.6, 7941.7)
020	J092720.29+101627.0	1.929	1740-53050-0065	3319-54915-0425	46.74	9.43 ± 0.06	0.16	-1.19 ± 0.35	(6004.7, 4842.5)
021	J093548.50+363121.9	2.977	1275-52996-0145	3223-54865-0303	47.10	–	–	$+10.56 \pm 0.91$	(19951.1, 17820.4); (16270.8, 11234.6); (9491.3, 7941.7)
022	J094602.23+380059.3	2.068	1276-53035-0160	3223-54865-0566	46.84	9.38 ± 0.19	0.23	$+2.95 \pm 0.38$	(18207.8, 16270.8);(9297.6, 8135.4)
023	J095901.24+550408.2	2.180	0945-52652-0436	3169-54821-0627	46.79	9.61 ± 0.12	0.12	-5.10 ± 0.49	(10459.8, 4261.4)
024	J100716.69+030438.6	2.124	0501-52235-0606	3257-54888-0474	47.10	9.42 ± 0.36	0.38	$+4.37 \pm 0.28$	(20725.9, 19176.3); (18788.9, 16270.8)
025	J101542.04+430455.6	2.420	1218-52709-0514	3287-54941-0433	47.48	–	–	$+5.35 \pm 0.24$	(8716.5, 6198.4); (5423.6, 3680.3)
026	J101616.34+383817.3	1.953	1427-52996-0479	3262-54884-0356	46.38	9.06 ± 0.21	0.17	$+6.01 \pm 0.65$	(25374.7, 23437.7); (21694.4, 19563.7); (19176.3, 17820.4)
027	J102754.03+182221.6	3.078	2591-54140-0453	2868-54451-0518	47.13	–	–	$+1.10 \pm 0.28$	(13171.6, 11815.7)
028	J110208.59+660156.5	2.064	0490-51929-0142	3171-54862-0164	46.59	9.10 ± 0.25	0.25	-4.90 ± 0.52	(16851.9, 15689.7); (15302.3, 12396.8)
029	J112239.20+602012.3	2.227	0951-52398-0523	3328-54964-0081	46.66	9.29 ± 0.15	0.19	-4.66 ± 0.61	(22275.5, 18788.9)
030	J112258.77+164540.3	3.031	2499-54176-0308	3327-54951-0153	47.35	–	–	$+1.31 \pm 0.20$	(19757.4, 18401.5); (8135.4, 7166.9)
031	J112703.06+450516.4	1.857	1366-53063-0321	3215-54861-0399	46.67	9.47 ± 0.14	0.13	-2.89 ± 0.42	(5617.3, 4648.8); (1937.0, 774.8)
032	J120653.39+492919.3	1.845	0969-52442-0107	2919-54537-0170	47.08	9.65 ± 0.05	0.22	-1.70 ± 0.25	(22662.9, 21500.7); (10847.2, 9297.6)
033	J120822.25+302423.9	2.252	2230-53799-0353	3181-54860-0025	47.18	–	–	-1.29 ± 0.28	(18014.1, 17045.6); (14140.1, 13171.6)
034	J121147.38+203402.4	2.413	2610-54476-0341	2918-54554-0622	47.00	–	–	-6.04 ± 0.52	(22081.8, 21113.3); (13365.3, 10653.5); (10266.1, 7360.6); (6198.4, 5229.9)
035	J122604.28+034317.8	1.767	0519-52283-0565	3253-54941-0202	47.12	9.63 ± 0.07	0.25	$+1.01 \pm 0.20$	(12009.4, 10653.5)
036	J123736.42+143640.1	2.704	1768-53442-0038	3254-54889-0548	46.83	–	–	$+0.98 \pm 0.27$	(22275.5, 21307.0)
037	J130136.12+000157.9	1.783	0293-51994-0074	0293-51689-0079	47.16	9.83 ± 0.08	0.17	$+0.41 \pm 0.12$	(13752.7, 12396.8)
038	J131433.83+032321.9	2.255	0525-52029-0572	0525-52295-0576	46.93	–	–	$+3.34 \pm 0.45$	(7360.6, 6004.7); (4842.5, 3874.0)
039	J131505.89+590157.5	1.932	0958-52410-0157	3237-54883-0067	47.10	9.69 ± 0.05	0.20	-2.47 ± 0.32	(10459.8, 7941.7); (4067.7, 2905.5)
040	J135721.77+005501.1	1.997	0301-51942-0408	0301-51641-0411	47.03	9.39 ± 0.11	0.34	-2.94 ± 0.36	(26149.5, 23050.3)
041	J143117.07+632701.7	1.891	0499-51988-0105	2947-54533-0370	47.17	9.62 ± 0.06	0.28	-1.29 ± 0.29	(18595.2, 16851.9)
042	J150033.52+003353.6	2.438	0310-51616-0363	0310-51990-0388	46.68	–	–	$+7.25 \pm 0.58$	(21500.7, 20338.5); (19370.0, 14140.1)
043	J232840.99-085315.8	1.729	0646-52523-0446	3145-54801-0367	46.69	9.43 ± 0.06	0.14	-2.21 ± 0.47	(14721.2, 13365.3)